Die approbierte Originalversion dieser Diplom-/Masterarbeit ist an der Hauptbibliothek der Technischen Universität Wien aufgestellt (http://www.ub.tuwien.ac.at).

The approved original version of this diploma or master thesis is available at the main library of the Vienna University of Technology (http://www.ub.tuwien.ac.at/englweb/).

TECHNISCHE UNIVERSITÄT WIEN

VIENNA UNIVERSITY OF TECHNOLOGY

M A S T E R A R B E I T

Finite Element Modelling of Radiofrequency and Microwave Liver Tumor Ablation

Ausgeführt am Institut für
Analysis & Scientific Computing
der Technischen Universität Wien

unter der Anleitung von
Ao.Univ.Prof. DDDr. Frank Rattay

durch
Wolfgang Schramm
Anton Figdor-Weg 3/1/17
A-2320 Schwechat

Ort, Datum

Unterschrift

Kurzfassung

Radiofrequenz ablation (RFA) ist eine minimal invasive Methode um mithilfe von Hitze pathologisches Gewebe wie z.B. Tumorgewebe zu zerstören. Bei einer RFA wird ein Applikator direkt in den Tumor eingeführt wo eine Koagulationsnekrose erzeugt wird. Während einer typischen Anwendung von 10 bis 15 Minuten wird eine ca. 3-5.5 cm große Sphäre an totem Gewebe erzeugt. RFA wird derzeit für thermische Ablation von Knochen, Leber, Nieren, Herz, Prostata, Brust, Gehirn und Tumorgewebe eingesetzt. Allerdings variiert die Menge an thermischer Energie die benötigt wird um eine komplette Nekrose zu erzielen. Dies liegt vor allem daran, dass viele Gewebeparameter zu wenig bekannt sind. Derzeit wird RFA aufgrund von empirisch gefundenen Daten durchgeführt.

Meine Arbeit behandelt die Erstellung von Finite Element Modellen, die das thermische Verhalten von Radiofrequenz- und Mikrowellenablation (MWA) untersuchen. Der Hauptteil dieser Arbeit behandelt den Vergleich der Beteiligung von direkter Erwärmung, Wärmeleitung und Perfusion an der resultierenden Wärmeverteilung eines typischen Radfrequenz bzw. Mikrowellen Durchlaufs.

Ich habe Finite Element Modelle einer RF Elektrode (gekühlt, 17 gauge) und einer MW Antenne (Dipol, 13 gauge) erstellt. RFA wurde für eine 12 Minuten Dauer simuliert wobei die zugeführte Energie so kontrolliert wurde, dass die maximale Temperatur ungefähr bei 100°C liegt. MWA wurde für eine Dauer von 6 Minuten simuliert, die zugeführte Energie betrug dabei 75W. Bei beiden Modellen wurde sowohl die Veränderung von elektrischen und thermischen Gewebsparameter also auch die temperaturbedingte Veränderung der Blutperfusion berücksichtigt. Bei beiden Simulationen wurde die Gewebstemperatur und den berechneten Perfusionseffekt ermittelt und evaluiert.

Die maximale Gewebstemperatur lag bei 100°C für die RFA und bei 177°C für die MWA. Bei beiden Modellen wird das Gewebe nur in Nähe des Applikators direkt erhitzt. MWA ermöglicht höhere Temperaturen als RFA, da Mikrowellen durch Gewebsaustrocknung und Verkohlung nicht limitiert werden. Durch höhere Temperaturen und einer geringeren Anwendungszeit ist MWA geringer durch Perfusion beeinflusst.

Abstract

In radiofrequency ablation (RFA) heat is generated locally by a high frequency, alternating current that flows from the electrodes inserted into the center of a tumor. The local heat that is generated melts the tissue (coagulative necrosis) that is adjacent to the probe. Within a time period of 10 to 15 minutes, the local heating will result in a 3 cm to 5.5 cm sphere of dead tissue per treatment. RFA so far has been widely used for thermal ablation in bone, liver, kidney, heart, prostate, breast, brain, and soft tissue tumors. However, the amount of thermal energy necessary to achieve a complete necrosis varies among many tissue parameters.

My work deals with the creation of finite element models describing such an ablation process and evaluating the various results. The main part deals with the comparison of the influence of direct heating, thermal conduction and perfusion on the heating pattern of a typical radiofrequency and microwave ablation session.

I created Finite Element computer models of a RF electrode (Cooled needle, 17 gauge), and a Microwave (MW) antenna (Dipole, 13 gauge). I simulated RF ablation for 12 min with power controlled to keep maximum tissue temperature at $100°C$, and Microwave ablation (MWA) for 6 min with 75W of power applied. For both models I considered change in electric and thermal tissue properties as well as perfusion depending on tissue temperature. I determined the tissue temperature profile at the end of the ablation procedure and the calculated effect of perfusion on both RF and MW ablation.

Maximum tissue temperature was $100°C$ for RF ablation, and $177°C$ for MWA. Lesion shape was ellipsoid for RF, and tear-drop shaped for MWA. MWA is less affected by tissue perfusion mainly due to the shorter ablation time and higher tissue temperature, but not due to providing deeper heating than RF. Both MW and RF applicators only produce significant direct heating within mm of the applicator, with most of the ablation zone created by thermal conduction.

Both RF and MW applicators only directly heat tissue in close proximity of the applicators. MWA allows for higher tissue temperatures than RF since MW propagation is not limited by tissue desiccation and charring. Higher temperatures coupled with lower treatment times result in reduced effects of perfusion on MWA.

Acknowledgement

I would like to thank everyone who helped me to make this thesis possible by their personal encouragement or technical advice. Particularly I want to thank:

- My supervisor Prof. Dr. Dieter Haemmerich at the Medical University of South Carolina for his endless optimism, his constant helpful advice and helping me to grasp the basic ropes of science.
- My supervisor Prof. DDDr. Frank Rattay at the University of Technology in Vienna for his constant advice.
- My parents Inge and Wolfgang and my brother Philipp for supporting and encouraging my studies and giving me the abilities achieve my goals in life.
- My girlfriend Bianca Schneeberger for constantly supporting me and for being on my side, even if that meant to live several thousand miles apart.
- My friends and colleagues at the Medical University of South Carolina and Vienna University of Technology for the enjoyable and memorable time.

Contents

1 Introduction **1**

2 Overview of Thermal Ablation Therapy **3**

2.1 Introduction 3

2.2 Methods of Thermal Ablation 3

2.2.1 Theoretical Background 3

2.2.2 Radiofrequency Ablation 5

2.2.3 Microwave Ablation 7

2.2.4 Clinical Devices for Tumor Ablation 7

3 The Liver **9**

3.1 Functional Anatomy 9

3.2 Cancer of the liver 11

4 Overview of Finite Element Analysis **18**

4.1 Introduction 18

4.1.1 Defining the "Problem Domain" 18

4.1.2 Pre-Processing 19

4.1.3 Solving 20

4.1.4 Post-Processing 20

4.2 Mathematical and Modelling Background 22

4.2.1 Mathematical Background 22

4.2.2 Modelling Background 23

4.2.3 Summary 25

4.3 Software Packages 25

4.4 Example Case 26

4.4.1 Pre-Processing in MSC Patran 2005 R2 26

4.4.2 Solving in Abaqus 6.5-1 30

4.4.3 Post-Processing 33

5 Relative Contribution of Thermal Conduction and Direct Heating During Tumor Ablation **35**
5.1 Summary . . . 35
5.2 Introduction . . . 36
5.3 Methodology . . . 37
5.3.1 RF-Model (RFM): . . . 37
5.3.2 RFM Tissue properties: . . . 37
5.3.3 Microwave-Model (MWM): . . . 37
5.3.4 MWM Tissue properties: . . . 38
5.3.5 Coagulation Zone Boundary: . . . 40
5.4 Results . . . 40
5.5 Discussion . . . 41
5.6 Conclusions . . . 53

6 Conclusion **54**
6.1 Summary . . . 54
6.2 Outlook . . . 54

A Bibliography **57**

B Sample Abaqus Input-File **62**

C User Defined routines **68**

Nomenclature

FEA	Finite Element analysis
FEM	Finite Element modelling
HBV	Hepatitis B Virus
HCC	Hepatocellular carcinoma - liver tumor
HCV	Hepatitis C Virus
MW	Microwave
MWA	Microwave ablation
RF	Radiofrequency
RFA	Radiofrequency ablation

Chapter 1

Introduction

During my work at the Medical University of South Carolina under the supervision of Prof. Haemmerich, I was involved in different projects dealing with Finite Element Modeling (FEM) of various tissue ablation techniques (predominately hepatic tissue). My work was done between September 2005 and September 2006. This thesis presents my work on quantifying the relative contribution of direct heating, thermal conduction and blood perfusion in Radiofrequency and Microwave heating. The concept of thermal ablation, either through heating or cooling, has evolved to be a very important tool in today's clinical environment. Possible treatments include:

- Heart Arrhythmias
- Enlarged Prostate
- Uterine Bleeding
- Tumor Ablation (e.g. Liver, Lung)

While all of these application areas are important for clinical medicine, my work concentrates on tumor ablation of liver tissue.
I will start with presenting an overview about thermal ablation in chapter 2. Then I will continue with giving a short introduction into the anatomy and physiology of the liver in chapter 3.
I will then start chapter 4 with a basic introduction into the mathematics and operation of FEA/FEM and conclude with the construction of the model I used for the main part of my research.
Chapter 5 presents my main research on the contribution of thermal conduction and direct heating during tumor ablation.

Finally I included a sample input file for the Abaqus solver in the Appendix.

The results obtained in chapter 5 were published in

Schramm W, Deshan Y, Wood B, Rattay F, Haemmerich D. *"Contribution of Direct Heating, Thermal Conduction and Perfusion during Radiofrequency and Microwave Ablation"*. The Open Biomedical Engineering Journal, 2007,1(1):47-52

Chapter 2

Overview of Thermal Ablation Therapy

2.1 Introduction

Thermal ablation therapy is a method of destroying (ablating) pathologic tissue (e.g. tumors) by either heating or freezing of the target tissue. There are six major methods currently in clinical use. Every method has its special field of use (see table: 2.1). Even tough surgical tumor resection stays the therapy of choice for resectable tumors, ablation therapy can increase the 5 year survival rate[1] for patients with non resectable tumors. Current clinical results show that these therapies provide better clinical results than chemotherapy or radiation therapy alone [11].

2.2 Methods of Thermal Ablation

2.2.1 Theoretical Background

Mathematical Background

Since thermal ablation is a method of destroying pathologic tissue with the use of temperature, we need a heat transfer equation suitable for the human (or animal) in-vivo environment. Pennes' Bioheat Equation provides us with the required mathematical foundation for that [44]:

[1]The *five year survival rate* gives the percentage of people who were diagnosed with cancer and were still alive after 5 years after the diagnosis. But it does not necessarily mean that the patients died after this 5 years, nor that they were cured.

Ablation modalities	RF	Cryo	Microwave	Ultrasound	Laser	Chemical
Cardiac ablation	***	**	*	*	N/A	N/A
Tumor ablation (liver, lung, kidney)	***	**	*	N/A	*	*
Endometrial	**	**	*	N/A	N/A	N/A
Prostate (cancer, enlarged prostate)	*	**	**	*	N/A	N/A
Intervertebral Disk	*	N/A	N/A	N/A	*	N/A
Endovascular	**	N/A	N/A	N/A	**	N/A
Cornea	**	N/A	N/A	N/A	***	N/A
*** used frequently ** used sometimes * used rarely/under investigation N/A not used clinically						

Table 2.1: Frequency of use of different ablation modalities in clinical applications [43].

$$\rho c \frac{\partial T}{\partial t} = \nabla \cdot k \nabla T + Q_A - Q_p \tag{2.1}$$

This mathematical fundament is well tested and widely used in the scientific community. The relation between the equation 2.1 and the real world scenario is as follows:

The applicator applies energy $Q_A(W/m^3)$ to heat or cool the target tissue. Some energy Q_p is carried away by blood perfusion. Depending on the target tissue Q_p can have a major influence on the outcome of the ablation process (e.g. hepatic tissue) or can be neglectable (cardiac tissue). According to Pennes' bioheat equation the effect of blood perfusion is modeled as a distributed heat sink term [43]:

$$Q_p = \rho_{bl} c_{bl} w_{bl} (T - T_{bl}) \tag{2.2}$$

where $\rho_{bl}[kg/m^3]$ denotes the density of blood and $c_{bl}[J/kg \cdot K], T_{bl}$ are the specific heat and the temperature of blood respectively [2]. $\rho c \frac{\partial T}{\partial t}$ describes how the tissue temperature T changes depending on the specific heat c and the density ρ of the tissue. $\nabla \cdot k \nabla T$ describes how thermal energy is conducted through the tissue, depending on thermal conductivity k [43]. The resulting

[2]Common values assumed for these parameters are: $\rho_{bl} = 1060[kg/m^3]$,$c_{bl} = 3780[J/kg]$ and $T_{bl} = 37°C$

area of tissue death is usually called *thermal lesion*, or *coagulation zone* for heat-based methods.

Thermal Tissue Injury

The aim the various ablation techniques is to destroy a certain area in the tissue (the so called coagulation zone) either due to thermal injury (e.g. RF-Ablation) or due to chemical interaction (e.g. Ethanol Ablation). Figure 2.1 shows a typical coagulation zone in liver tissue right after RF ablation.

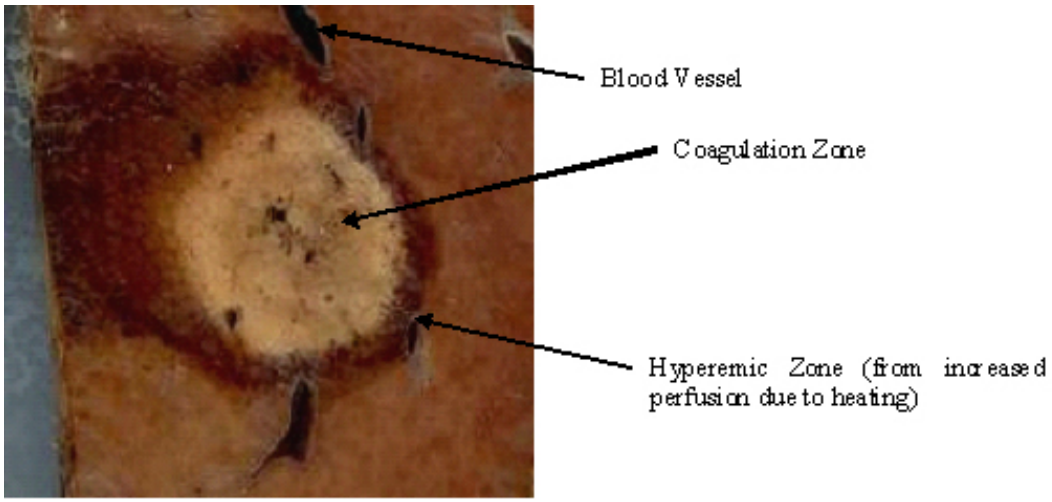

Figure 2.1: Gross pathology of a coagulation zone created by RF ablation in vivo in porcine liver. Liver was sliced right after the ablation procedure.

2.2.2 Radiofrequency Ablation

For a RF ablation therapy an applicator is inserted into the tumor. Then RF current in the frequency range of 450 - 500kHz is applied to the tissue. The current is carried through the tissue through ions (mainly Sodium, Chloride and Potassium). The ions oscillate due to the alternating electric field, resulting in resistive heating (Joule Heating) due to ionic friction [43]. Most heat is usually generated close to the tip of the electrode since this is the area of the highest RF current density. On the first sight it appears to be fairly straight forward to produce a coagulation zone of the desired size, but there are several factórs limiting the maximum temperature which can be achieved by RF ablation, and so limiting the maximum coagulation zone:

- Tissue charring: Charring of the tissue occurs around the electrode if too much RF power is applied. The charred tissue is electrically insulating

and typical irreversible.

- Vapor: At temperatures around $\approx 110°C$ the water in the tissue vaporizes and builds a electrically insulating barrier. This process is reversible.
- Energy loss: In tissue, energy is permanently removed by perfusion. This effect can be neglectable, or can have a major influence on the outcome of a therapeutic session.

Therefore the applied power and temperature has to be controlled. At the moment there are three different control methods in commercial available RF Devices:

- **Power Control:** Applied RF power is constant throughout the ablation process.
- **Temperature Control:** One or more thermal sensors are embedded in the catheter tip or at a certain distance from the catheter. Applied RF power is controlled to maintain the tissue temperature at the sensor constant at a certain level.
- **Impedance Control:** Applied RF Power is controlled via the tissue impedance between the active electrode and the grounding pad.

Various possibilities do exist to modify the thermal properties of the tumor tissue to influence the aforementioned limitations to be able to yield a better performance [32, 2, 4]:

- Change thermal and/or electrical tissue conductivity
- Reduce tumor perfusion
- Synergistic toxicity with cellular hypoxia or pre-treatment with radio or chemotherapy

While the current goal in research is to maximize the coagulation volume, little research has been done on how to influence the shape of the coagulation zone. In my opinion this is important for treatment locations where the preservation of adjoining anatomical structures is essential (e.g. the Diaphragm). Several strategies have been proposed how to handle a "safe" procedure close to important anatomical regions, but as mentioned before, little research has been done on how to preserve those structures with influencing the resulting shape of the coagulation zone.

2.2.3 Microwave Ablation

Microwave tumor ablation is still a fairly new technology currently used in various clinical trials but is so far not used in daily use. The principles are essentialy the same as for RFA, but since microwave heating is not subject to the limitations of stem buildup and tissue charring as RFA, it seems likely that with higher treatment temperatures also greater volume coagulation zones may be achievable (see also chapter 5).

2.2.4 Clinical Devices for Tumor Ablation

The following commercial devices are currently available for hepatic tumor ablation [35]:

Radiofrequency Ablation:

These devices use applied power between 200 - 250W, application times of 12 - 45 minutes and create coagulation zones of 3-6 cm in diameter. All manufacturers use different electrodes, and algorithms to control the applied power [43].

RITA medical: Rita medical[3] manufactures the Starburst and Habib series for RF-ablation. (see 2.2a)

Boston scientific: Boston scientific[4] produces the LeVeen needle system for RF-ablation.(see 2.2b)

Valleylab: Valleylab[5] manufactures the Cooltip series for RF-ablation. (see 2.2c)

Microwave Ablation:

Until recently MWA has only be used for small tumors in the Asian region. Vivant Medical of Mountain View, CA) currently plans to release a MWA system to the american market in the newar future. The advantage of MWA over RFA are shorter treatment times, higher treatment temperatures due to the fact that MWA is not affected by tissue charring (see also chapter 5).

[3] http://www.ritamedical.com
[4] http://www.bostonscientific.com
[5] http://www.valleylab.com/

Figure 2.2: RF electrodes of three manufacturers currently commercially available, and in clinical use. Multi-prong electrodes by RITA medical (a), and Boston Scientific (b). Cooled needle electrode (single and triple-cluster) by ValleyLab (c) [43].

Cryo Ablation:

Even though my work doesn't involve the use of Cryoablation, I mention it for the sake of completeness. Until recently Cryoablation has been only performed during open surgery, recently however devices for minimal invasive treatment have become available. Current Cryoablation devices usually use liquid Nitrogen or Argon cooling systems for freezing the tissue. One of the main advantages of Cryoablation is the possibility of real-time monitoring of the procedure, since the formed iceball is visible under ultrasound.

Chapter 3

The Liver

3.1 Functional Anatomy

The liver is the second largest organ of the human body. Its usual weight is between 1kg and 1.5kg and represents 1.5% to 2.5% of the lean body mass [26]. Its function is to process the nutrients absorbed in the digestive tract and to store them for use by other organs. The liver is located in the right upper quadrant of the abdomen under the right lower rib cage against the diaphragm and projects for a variable extent into the left upper quadrant. The liver is attached to the diaphragm, peritoneum, great vessels, and upper gastrointestinal organs. The liver has two major blood supplies [12]:

- The portal vein arising from the stomach, pancreas, intestines and the spleen transports nutrient rich blood. It accounts for 80% of the blood supply.
- The hepatic artery, transporting oxygen rich blood accounts for 20% of the blood supply.

The most important function of the liver is to filter the blood coming in from the Gastrointestinal (GI-)tract and the rest of the body[12]. Other important Functions of the Liver:

- Formation and secretion of bile
- Nutrient and vitamin metabolism
- Inactivation of various substances
- Synthesis of plasma proteins

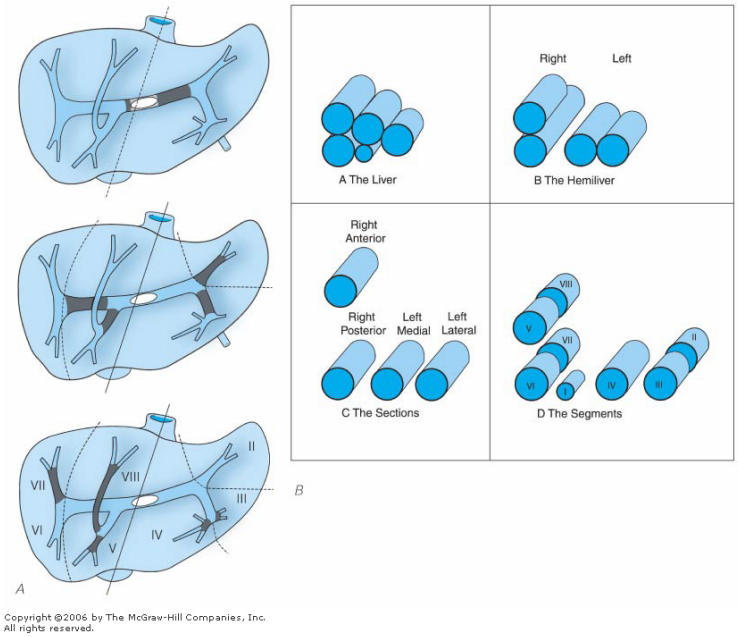

Figure 3.1: A. Primary, secondary, and tertiary bifurcations of the portal pedicle as seen from the cephalad aspect of the liver. B. The liver lobes, sectors/sections, and segments are viewed as cylinders. The hemilivers are separated by the middle hepatic vein plane and are supplied by the primary branches of the main portal vein. The sections/sectors are divided by the right and left hepatic veins and are supplied by the secondary portal bifurcation within each lobe. The segments are supplied by the tertiary branches (bifurcation within a section/sector) and split along the coronal plane of the main portal bifurcation [42].

- Immunity

The basic building block of it is the liver cell (hepatocyte). A hepatocyte is a epithelial cell and is grouped in interconnected plates. Hepatocytes make up for two-third of the liver mass [27]. The structural units of the liver are called liver lobules. The liver lobule is formed of a polygonal mass of tissue about 0.7 x 2 mm in size, with portal spaces at the periphery and a vein, called the central or centrolobular vein, in the center (see Figures: 3.1, 3.2, 3.3) [27]. The hepatocytes are arranged in ways resembling a brick wall, this structure and the typical consistency of the cellular plates form a spongelike structure. An important factor in the surgical treatment of the liver is the ability to restore/replace the removed tissue. The liver has an extraordinary capability to restore itself after removal of hepatic tissue, despite the slow rate of cell renewal. The regenerated liver tissue is normally well organized, has the typical lobule arrangement and is able to replace the functions of the removed tissue. However, if the tissue is continuously damaged (e.g. in alcohol misuse[1]) the multiplication of liver cells is followed by an increased amount of connective tissue. Instead of functional hepatic tissue, a mass of unorganized hepatocytes surrounded by connective tissue very rich in collagenous fibers is formed[2] (see Figure: 3.4). [27]

3.2 Cancer of the liver

Neoplasia (Latin, new growth) in general is an abnormality of cellular differentiation and control of growth. The term "tumor" is most commonly used to denote a formation of masses of abnormal tissue (neoplasms). Tumors are being categorized in benign and malignant tumors depending on various characterizations. In short, a benign neoplasm can grow, but does not have the ability to spread from the site of origin to other parts of the body, in contrast a malign neoplasm grows and can spread from the origin through different ways to other sites of the body (metastasize). The term "cancer" denotes a malignant neoplasm. There is also a third kind of neoplasm, which is local invasive, but has only low metastatic potential (see figure: 3.5) . Those are most commonly referred to as locally aggressive neoplasms or low-grade malignant neoplasms [7]. Rupert Willis defines the process of Neoplasia in this way [7]:

[1] Ethanol is primarily metabolized in the liver. The main problem of the metabolization of ethanol is, that ethanol changes the hepatic regeneration in a (currently) unknown process, so it favors the development of cirrhosis.

[2] This disorder is called liver cirrhosis

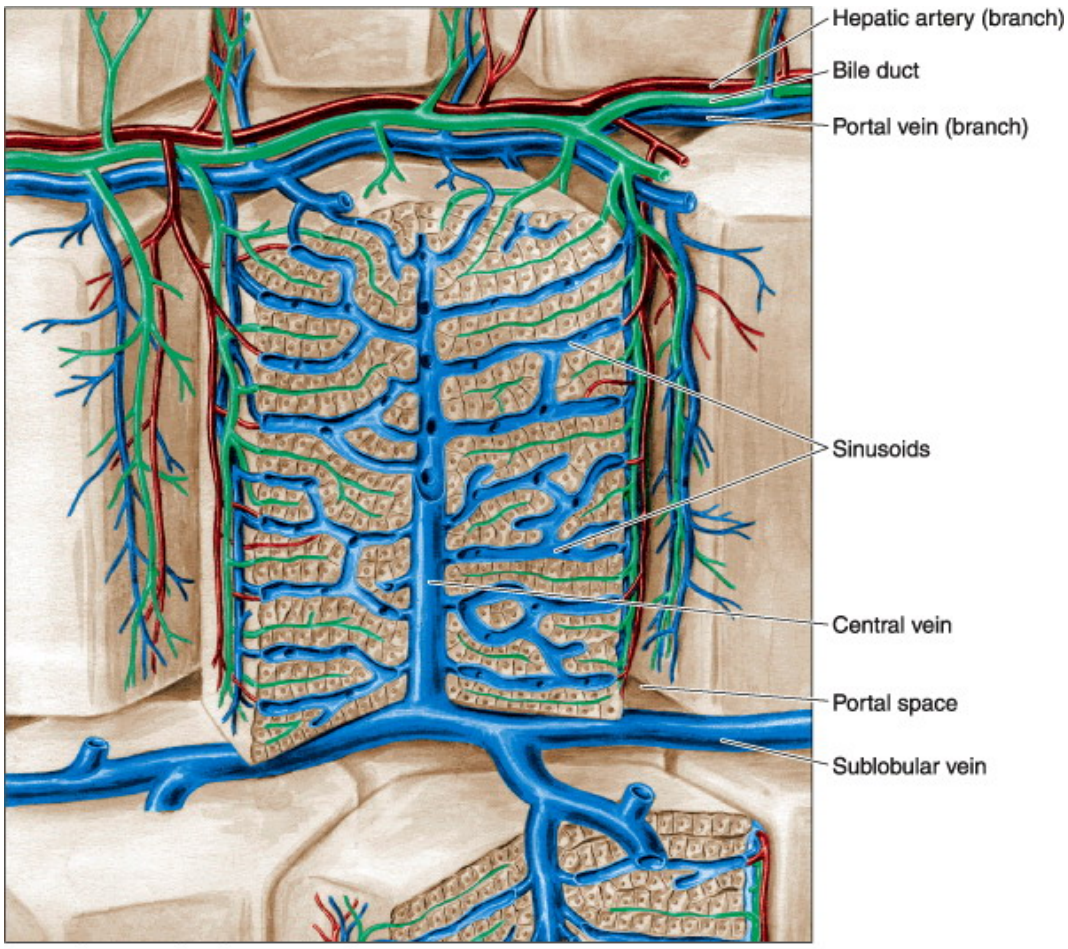

Copyright ©2006 by The McGraw-Hill Companies, Inc.
All rights reserved.

Figure 3.2: Schematic drawing of the structure of the liver. The liver lobule in the center is surrounded by the portal space (dilated here for clarity). Arteries, veins, and bile ducts occupy the portal spaces Nerves, connective tissue, and lymphatic vessels are also present but are (for clarity) not shown in this illustration. In the lobule, note the radial disposition of the plates formed by hepatocytes; the sinusoidal capillaries separate the plates. The bile canaliculi can be seen between the hepatocytes. The sublobular (intercalated) veins drain blood from the lobules [6].

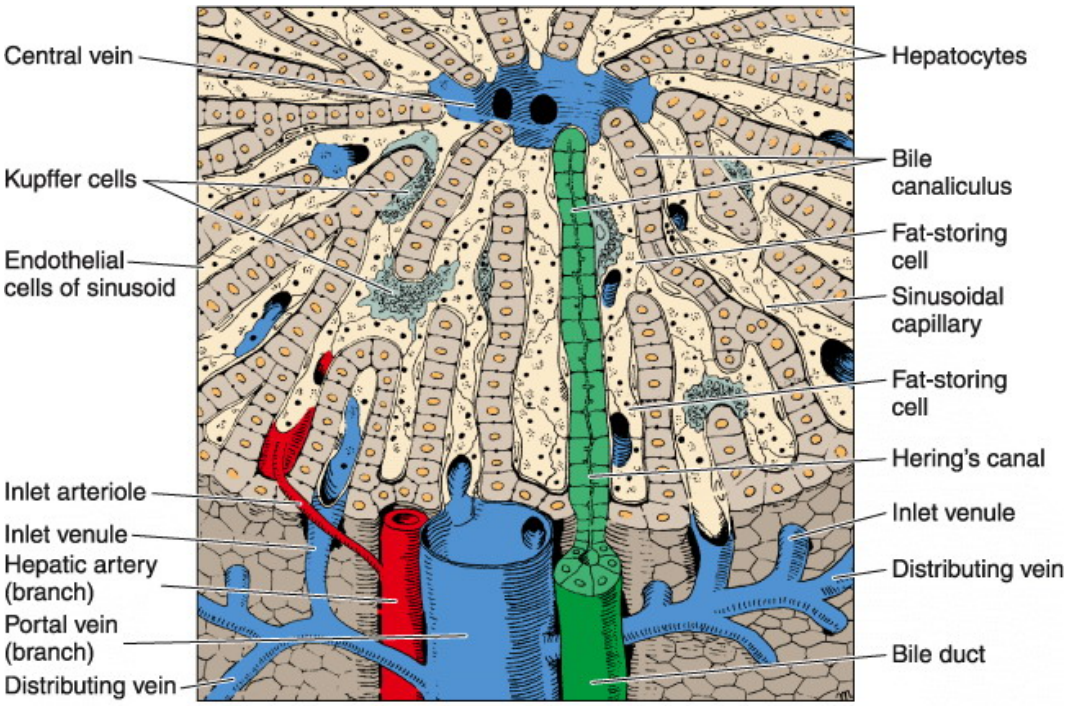

Copyright ©2006 by The McGraw-Hill Companies, Inc.
All rights reserved.

Figure 3.3: Three-dimensional aspect of the normal liver. In the upper center is the central vein; in the lower center is the portal vein. Note the bile canaliculus, liver plates, Hering's canal, Kupffer cells, sinusoid, fat-storing cell, and sinusoid endothelial cells. (Courtesy of M Muto.)

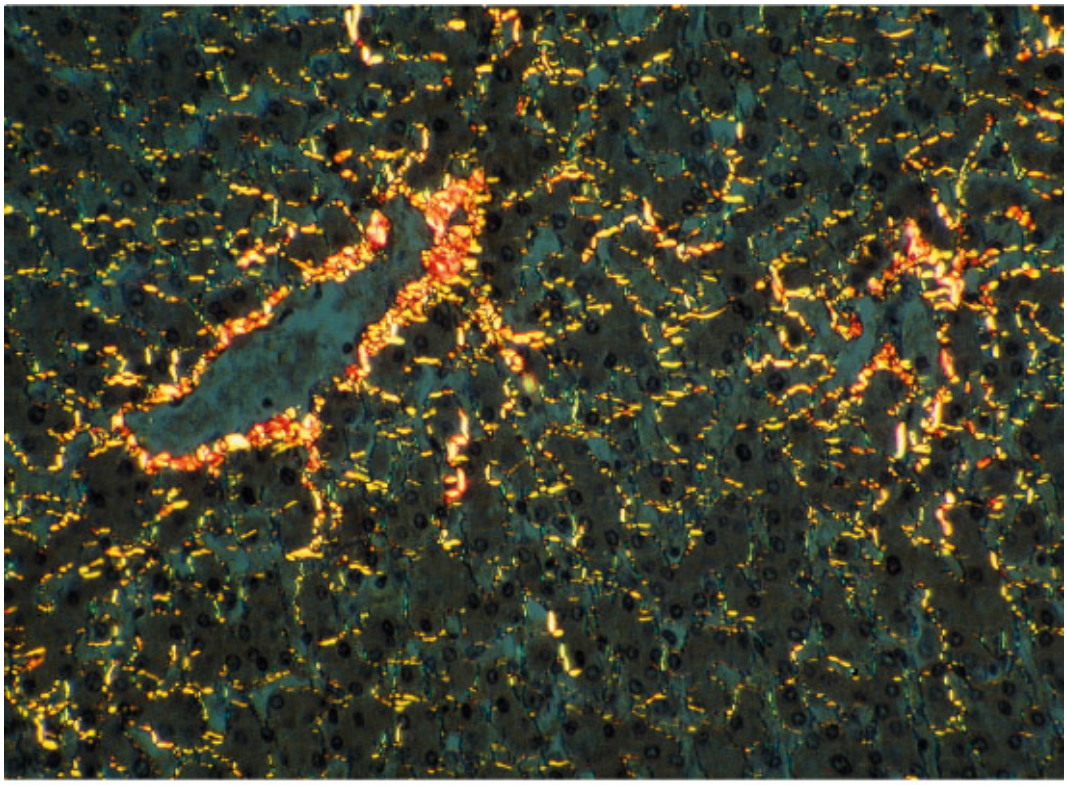

Copyright ©2006 by The McGraw-Hill Companies, Inc.
All rights reserved.

Figure 3.4: Section of human liver with cirrhosis induced by the local inflammatory action of the eggs of a nematode (Schistosoma). Collagen content was increased severalfold, resulting in circulatory disturbance. Picrosirius stain and polarizing microscopy. Medium magnification [27].

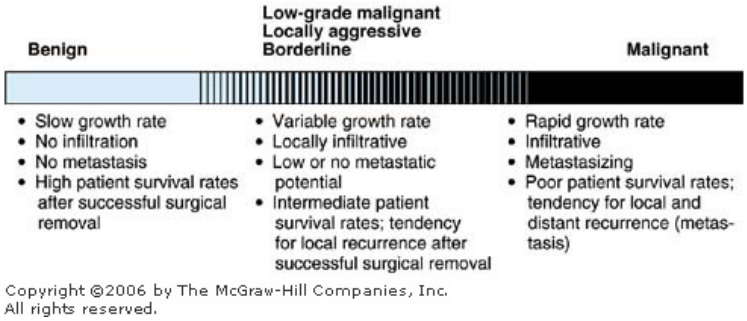

Figure 3.5: Biologic behavior of neoplasms. The behavior of neoplasms is shown as a spectrum from benign to highly malignant. There is also an intermediate group of low-grade malignant neoplasms composed of those that have the potential for local recurrence but limited or no metastatic potential.

> 'A neoplasm is an abnormal mass of tissue, the growth of which exceeds and is uncoordinated with that of the surrounding normal tissues and persists in the same excessive manner after cessation of the stimuli that evoked the change.'

Table 3.1 lists the most important features for tumors evaluation[3]. Primary and secondary malignant hepatic tumors belong to the most common cancers worldwide, but chemotherapy and radiation therapy are usually ineffective for treatment of those tumors [11].

Benign	**Malign**
Gross Features	
Smooth surface with a fibrotic capsule; compressed surrounding tissues.	Irregular surface without encapsulation; destruction of surrounding tissues.
Small to large, sometimes very large.	Small to large.
Slow rate of growth.	Rapid rate of growth.
Rarely fatal (except in central nervous system) even if untreated.	Usually fatal if untreated.
Microscopic Features	
Growth by compression of surrounding tissue.	Growth by invasion of surrounding tissue.

[3]None of these features is absolute; metastasis, invasion, and anaplasia are the most helpful.

Benign	**Malign**
Highly differentiated, resembling normal tissue of origin microscopically.	Well or poorly differentiated. Most malignant neoplasms do not resemble the normal tissue of origin (anaplasia).
Cells similar to normal and resembling one another, presenting a uniform appearance.	Cytologic abnormalities [4] including enlarged, hyperchromatic, irregular nuclei with large nucleoli; marked variation in size and shape of cells (pleomorphism).
Few mitotic figures [5] those present are normal.	Increased miotic activity; abnormal, bizarre mitotic figures often present.
Wellformed blood vessels.	Blood vessels numerous and poorly formed; some lack endothelial lining.
Necrosis unusual; other degenerative changes may be present.	Necrosis and hemorrhage common.
Distant spread (metastasis) does not occur.	Metastasis to distant sites.
Investigative techniques	
DNA content usually normal.	DNA content of cells increased, additional chromosomes commonly present.
Karyotype usually normal.	Aneuploidy, polyploidy, clonal genetic abnormalities[6].

Table 3.1: Summary of features differentiating benign and malignant neoplasms

Primary tumors of the liver is one of the most common malignancies worldwide. The annual international incidence of the disease is some 1 million cases, with a male to female ratio of approximately 4:1. In the United States, approximately 15,400 new tumors of the liver and biliary passages are diagnosed each year, with 12,300 deaths estimated annually [34]. Primary HCCs account

[4]Note that the cytologic abnormalities of malignant neoplasms resemble those of dysplasia but are more extreme.

[5]Note that some nonneoplastic states have numerous mitotic figures (eg, normal bone marrow, lymph nodes undergoing an immune response).

[6]Subtle gene deletions or translocations are being recognized with increased frequency.

for approximatly 4000 - 6000 cases per year in the USA [39, 5]. This incidence rate may be underestimated, since there are about 4 million Hepatitis C Virus (HCV) carriers alone in the USA. From these HCV carrier, approximately 10% are likely to develop HCC. Since there are two more major predisposing factors for HCC, namely hepatitis B (HBV) infection and chronic alcohol abuse, a much higher incidence for HCC seems more likely (current estimates: 60000 new HCC cases annually) [9].

The liver is also very susceptible to metastases from predominately colorectal cancer and ocular melanoma. Liver metastases are often the sole life-limiting factor of patients diagnosed with various cancer types and is assotiated with a poor prognosis. Since there are many factors that can cause metastases in the liver the actual incidence for this type of cancer is approximately 20 times higher than the incidence for primary hepatic tumors [26].

Chapter 4

Overview of Finite Element Analysis

4.1 Introduction

Finite Element Modeling/Analysis (FEM/FEA) is the process of numerically solving various physical problems with the help of 1D, 2D or 3D geometry and the according differential equations. It was developed by Richard Courant in 1943 who used the Ritz method to calculate approximate solutions to vibration systems. One of the most popular use of FEM/FEA is the calculation of car crash deformations (stress analysis) in the automobile industry and the calculation of aeronautical parameters (e.g. flow dynamics) in the aerospace industry. Nowadays engineering is highly dependent on the ability to simulate complex processes in a computer environment. I used FEA to calculate heat transfer and electro-thermal coupled processes.

The following four steps are necessary to perform a Finite Element Analysis:

- Defining the "Problem Domain"
- Pre-Processing
- Solving
- Post-Processing

4.1.1 Defining the "Problem Domain"

Before starting analyzing your real life problem, you have to abstract it to a format usable by your Finite Element solver. That means you have to evaluate

the physical properties you have to calculate (in general that determines the type of solver you have to use). Furthermore you have to check if your plan is likely to yield the wanting results. This usually involves a lot of literature research and long discussions with your colleagues. An advantage of almost all of the FEA/FEM packages is, that you don't actually have to implement the various equation systems, but you still have to be able to decide which equations are to be used. In most cases it is sufficient to define the analysis type (e.g. coupled thermal-electrical analysis), the required equations are then chosen by the solver.

4.1.2 Pre-Processing

Pre-Processing is after the definition of the problem domain the most important step. Mistakes in this step, may have various unintended consequences ranging from results which are slightly off to results which are "not even wrong"[1] thus requires retracing your steps to the very beginning of the simulation process and redo the various simulation runs. Since a simulation can usually take up to several hours, redoing all of your work results fairly often in additional work related stress due to various time constraints.

The Pre-Processing step generally consists of the following tasks:

- Defining the 1D/2D/3D Geometry of the system
- Defining the materials and their properties which are going to be used in the simulation
- Defining the Finite Element mesh
- Preparing the model for import into the finite element solver program

Defining the geometry is the first task of abstracting a real world scenario into a computer model. Abstracting real world structures into a geometry suitable for analysis can range from a simple task like creating two adjacent squares in 2D to a fairly complex task involving creating complex structures in 3D. Generally it's impossible to capture an objects whole complexity, but for simulation purpose that's usually not needed. "Keeping it as simple as possible and as complex as necessary" is a good rule of thumb for model design.

[1] A famous quotation by the Austrian physicist Wolfgang Pauli

Defining the material properties is usually the second task in model design. As mentioned before Finite Element Analysis uses real world properties to simulate a scenario as accurately as possible. Therefore concise parameters of the involved materials are needed. The required parameters vary between different simulation scenario. In a typical architectural scenario where you have to calculate the stability of one or more buildings you need parameters describing the physical stability of the various building materials. There are various sources for obtaining those values.

Creating the Finite Element mesh is usually the step involving the most "trial and error" approaches. The aim of this step is to create the so called *Finite Element Mesh* based on the geometry created in the beginning. This mesh consists of *nodes* and *edges*. For more accurate results, especially if you only allow small changes in the sought variable a tight mesh creation is absolutely necessary. However, in most cases you don't need the same amount of accuracy in the various parts of your model. Therefore most of the commercially available Finite Element tools allow the creation of nonuniform meshes in order to reduce the needed computation time and the required memory for the solving process. See 4.4.1 for an example mesh.

Section 4.4.1 shows the Pre-Processing step on a small example which gives an overview about the aforementioned methods.

4.1.3 Solving

The solving part of the Finite Element model is used - as the name suggests - to produce a numerical solution for the defined problem.

4.1.4 Post-Processing

Post-Processing a solution is the process of analyzing the numerical solution obtained in the solving step. Most solver software packages (e.g. Abaqus) provide the possibility to visualize the various calculated variables (for an example see figure 4.1).

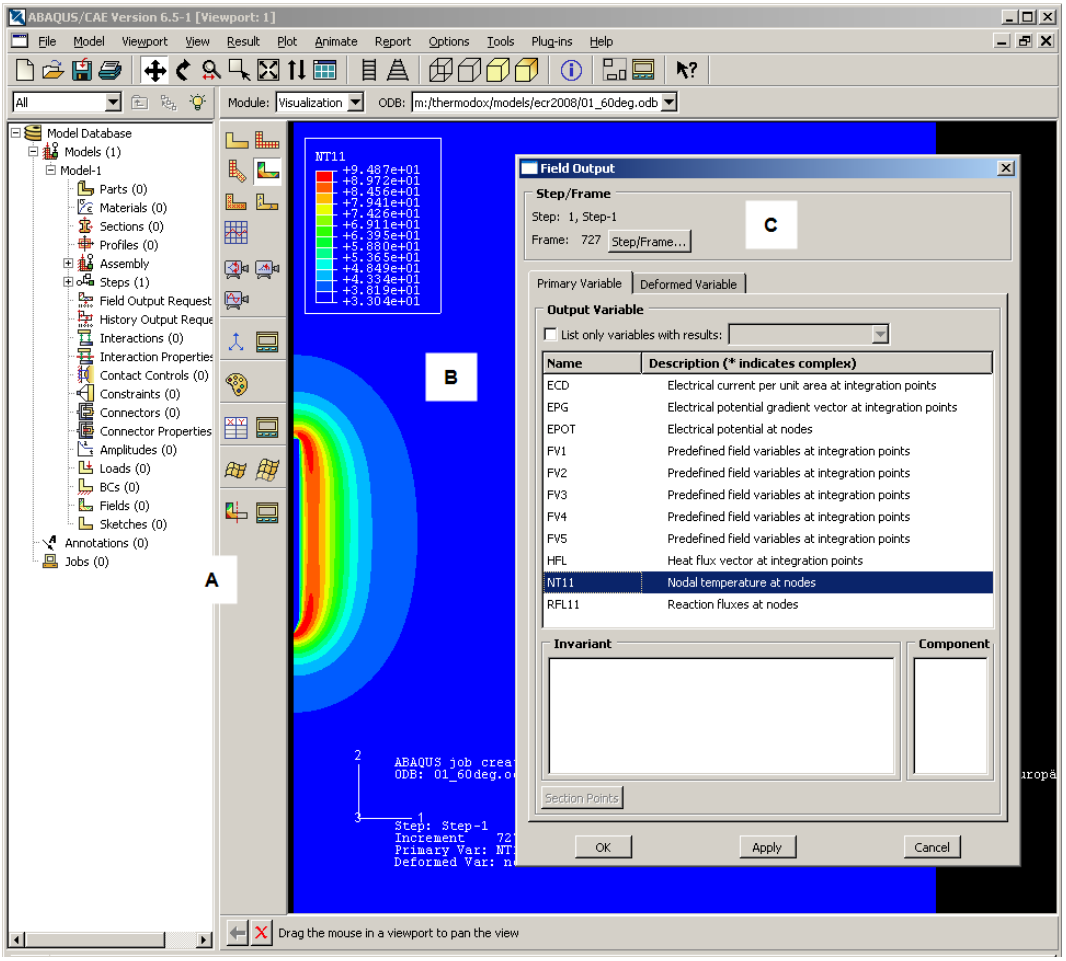

Figure 4.1: A: The model tree displaying the various elements of the model B: This area shows the visual representation of the selected solution variable - in this case the nodal temperature C: Shows the selection menu for the various solution variable

4.2 Mathematical and Modelling Background

4.2.1 Mathematical Background

There are generally two main approaches to solve the simultaneous equations for the desired variable at each node of the model. The first one is to use direct methods like LU decomposition or Gauss elimination. The second one is to use iterative methods e.h. Gauss-Jacobi or line relaxation method. Since direct methods work on fully assembled equation systems they a high storage capacity, thus these methods are usually only suitable for smaller models with up to 100.00 nodes. Iterative methods on the other hand are able to work on a partial assembled equations system, this gains a major reduction in needed storage capacity and is thus also suitable for large systems. In complex analysis scenarios usually non linear equations are involved which need to use another iterative loop. Since most simulations compute a solution over a prescribed time *time-stepping* is needed. This means, that the solution is found for an initial time and then subsequently computes the solution for other time points. When solving simulations with *time-stepping* you can choose either implicit approaches which result in a more accurate numerical solution but are very inefficient or you can employ explicit approaches which have a lower numerical stability but are more efficient [30].

The actual equations to use depend on several factors and are out of scope for this thesis. However I want to give a short overview of the different factors which are involved to obtain the final set of equations needed to compute the solution and the different approaches on how to solve such a system.

The first and most important factor is the physical domain the model is governed by and thus decide the type of analysis. The most common types of analysis are [1, 29]:

- Static stress analysis: A static stress analysis computes the deformation of an object where a static load is applied. A static load is a constant force operating on the object's surfaces and thus causing a deformation.
- Dynamic stress analysis: A dynamic stress analysis is different from a static one in the aspect the applied forces can vary (e.g. the influence of an earthquake on a building).
- Heat transfer and thermal-stress analysis: This is used to model heat conduction by conduction convection and radiation. The type of heat transfer used is highly dependent on the used element type.

- Electrical analysis: This can be used to perform a *coupled thermal-electrical* analysis to calculate the temperature rise in an object due to joule heating caused by energy dissipated by an electrical current. Or it can be used to so solve *piezoelectric* problems. Those are problems where the electrical potiential gradient causes straining and stress causes an electrical potential gradient.

Further factors include the chosen element type (see section 4.2.2), desired numerical accuracy and the available storage and computing capacity.

4.2.2 Modelling Background

When beginning a new project the problem of "where to start" often arises. Especially in a field where there is little to no experience the beginning can be a daunting task. As aforementioned mistakes in the design process can result in a high amount of retracing the modelling and model setup steps and redoing the simulations which usually take up to several hours - depending on the model complexity.
At this point I want to introduce my personal experience on starting with a new Finite Element project and so give a general idea on how to approach a more complex simulation (see the example case in 4.4) step by step from a simple model layout. To validate my initial assumption on how to design the basis for my model I decided to implement an 1D geometry instead of a 2D axi-symmetric or 3D geometry. Working with this simple model enabled me to adjust the load and boundary conditions in a way that the model is solvable and has a stable result. Figure 4.2 shows the simple geometry for a 1D heat transfer analysis.

After creating and validating the initial experiments the next step is to create a more complex model as simply as possible. Often you can use the general shape of the real world situation you want to simulate to simplify the model's geometry. The easiest way to do a simplification in such a case is if the object to be modeled has a cylindrical shape. It is possible to reduce a 3D cylinder into a 2D object by using a special element type provided by most commercial Finite Element solver. By defining the model *axi-symmetric* an independent axis is removed (usually the z-axis) and thus immensely reduces the needed computation cost. The result of course can also be interpreted for a three-dimensional case because you can assume the values along the "imaginary" z-axis equal to the values along the x-axis.

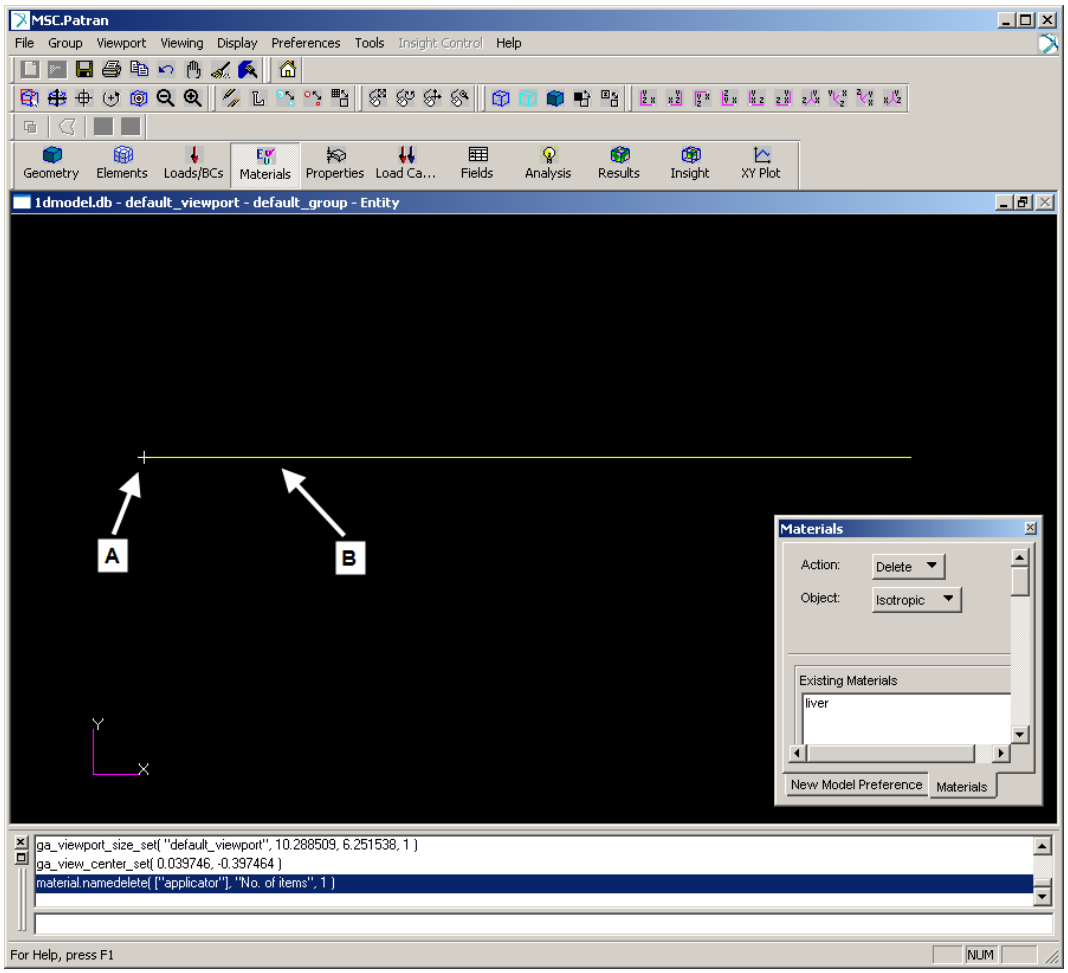

Figure 4.2: A: A single node acts as the source for the applied electrical energy; B: The rest of the geometry is assigned the liver material properties

This step wise approach allowed a time efficient development process. The initial 1D simulations took about 10 minutes to complete while the more complex 2D axi-symmetric model took about 2 hours to complete on a desktop workstation with a 2Ghz P4 and 2GB RAM running under WindowsXP.

It is essential to know the different element types that are useable by the chosen Finite Element solver. The most commonly used element types to describe the geometry are [30, 1]:

- 3D solids: As the name suggests, a 3D solid is a three-dimensional representation of a solid object (e.g. block of concrete). The object's surface is divided into two kinds of surfaces. One kind which where external forces are prescribed on. And one kind where displacements are prescribed.
- 2D solids: 2D solids are often used to simplify a 3D solid if it can be treated as a 2D solid. Since the transformation involves the removal of an axis it has to certain that the other two axis are independent of the axis to be removed.
- Rod: A rod is a 1D element type where the load and eventual boundary conditions are applied and evaluated along the prescribed axis.
- Further element types include truss, shell and beam elements

4.2.3 Summary

It is important to state that since there is such a magnitude of different factors influencing the approach on how to assemble and solve a set of differential equations or to approach the actual creation of the model, there are also a magnitude possible solutions on how to solve a certain problem. You usually have to decide if you implement an algorithm which has a higher numerical stability but suffers from inefficient computation, or if you choose to employ a much faster solution but have the risk of wrong results due to a lower numerical stability. Further it is advisable to start with a simple model where it is possible to verify the assumed model parameters, and then continue to a more sophisticated model where verification is much more difficult.

4.3 Software Packages

There are various industry grade products on the market for the purpose of *Finite Element Analysis* and *Finite Element Modelling*. While the usability

and the functionality of the various software packages is quite different, the naming conventions are interestingly quite similar between these programs. Some packages support the complete *Finite Element Modelling and Analysis* process (e.g. Abaqus), other packages specialize on just a subtask (e.g. solving or pre-processing). Under certain circumstances it is necessary to combine different products although each of them would support the complete process. That's why it is especially important to have a thorough overview over the various products and their capabilities and limitations.

The following list presents a small subset of the most important Finite Element tools currently available:

- ABAQUS[2]
- Comsol Multiphysics (formerly Comsol Femlab)[3]
- LSDYNA[4]
- MSC PATRAN[5]
- EDS IDEAS NX
- Altair Hypermesh (part of Altair Hyperworks)[6]

4.4 Example Case

Here I demonstrate the workflow for generating and solving the RF-ablation model I used for the main research project (see 5).

4.4.1 Pre-Processing in MSC Patran 2005 R2

Creating the Geometry

The first step is to create the basic geometry, which is the basis for the actual Finite Element Mesh. In my case, the geometry is quite simple, hence I only used some 2D primitives.

To reduce preparation time as well as calculation time, I decided to create my model 2D axi-symmetric. This was permitted due to the shape of the

[2]see: http://www.abaqus.com
[3]see: http://www.comsol.com
[4]see: http://www.lstc.com
[5]see: http://www.mscsoftware.com
[6]see: http://www.altair.com

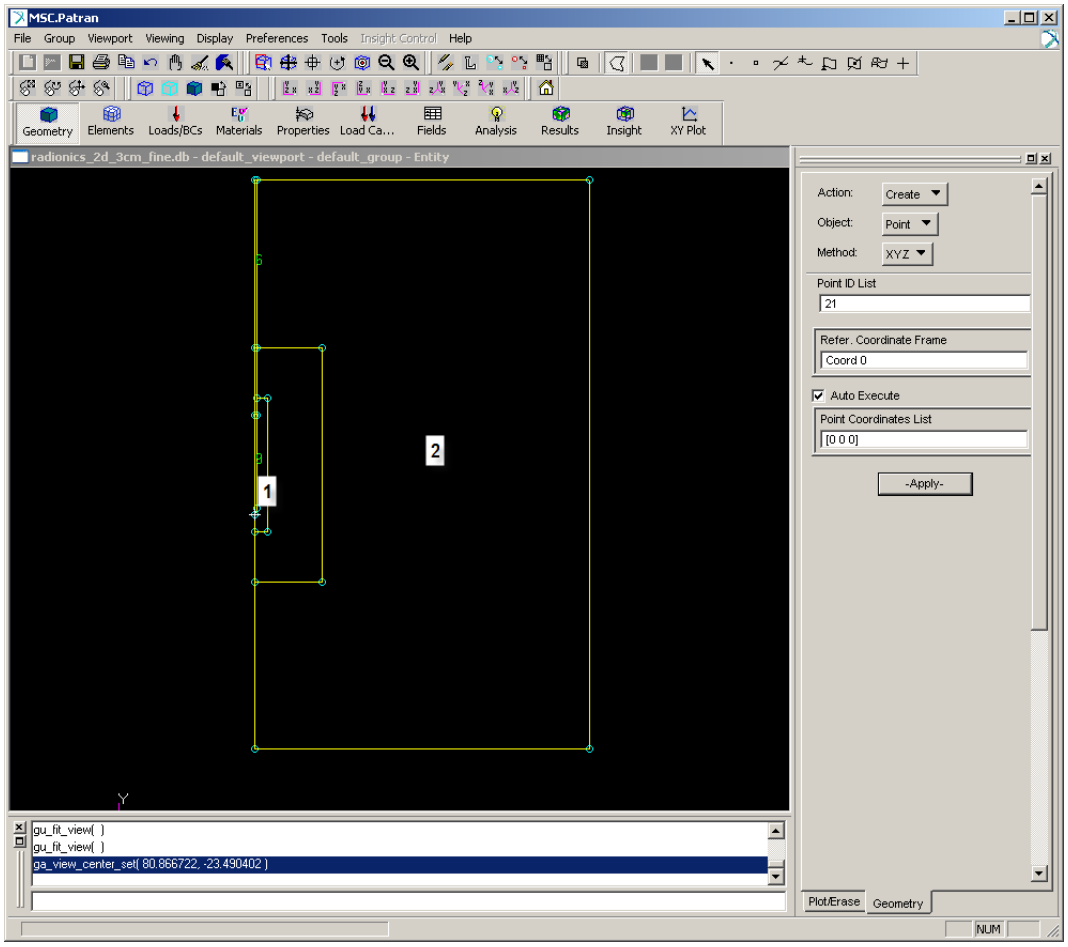

Figure 4.3: Basic Model Geometry. 1: The applicator area, 2: Liver tissue

applicator and is suggested by several publications so far (e.g. [25]). One big drawback of MSC Patran is its unintuitive user interface and its lack of multiple undo steps. Every change is automatically saved into the model, so you have to work out an exact plan how you want to develop your model. Figure 4.3 shows the final basic geometry for the model. The next step is define the material for each part of the model.

Defining the Material, Mesh and Boundary Conditions

I used three different materials in this model to create a simplified but still realistic simulation scenario.

- *PU_MAT*: for the insulated part of the applicator
- *FE_MAT*: for the active part of the applicator
- *LIV_MAT*: for the hepatic tissue.

ρ, kgm^3	1060
$c, J(kg * K)^-1$	3600
$k, W(m * K)^-1$	0.512
$\sigma, Sm^-1 at 50kHz$	0.333

Table 4.1: Hepatic tissue properties

These materials are based upon widely used values for a) an insulating material (in this case polyurethan); b) a highly conductive metal; c) the hepatic environment. These values were provided by my supervisor and are well published (e.g. [25, 23, 17]).

The material parameters used are:

- Density
- Electrical Conductivity
- Thermal Conductivity
- Specific Heat

Table 4.4.1 shows the used material properties for the liver tissue:

After defining the material you have to generate the Finite Element mesh. I decided to employ an non-uniform mesh which is tight close to the applicator and is becoming wider close to the edge. Since temperature differences will be higher close to the applicator I need a mesh which will provide more accurate results. Figure 4.4 shows the final mesh distribution.

When the mesh is generated I need to apply initial and boundary conditions and the applied load (in this case voltage) describing the physical environment for the simulation. The following parameters were applied:

- Initial Temperature: 37°C. This condition was applied in the whole model, since this is a safe value to assume for the core temperature of the liver.
- Outer Temperature: 37°C. This was applied along the edges of the model.
- Voltage: Initial energy output. This was applied along the electrical active part of the applicator.

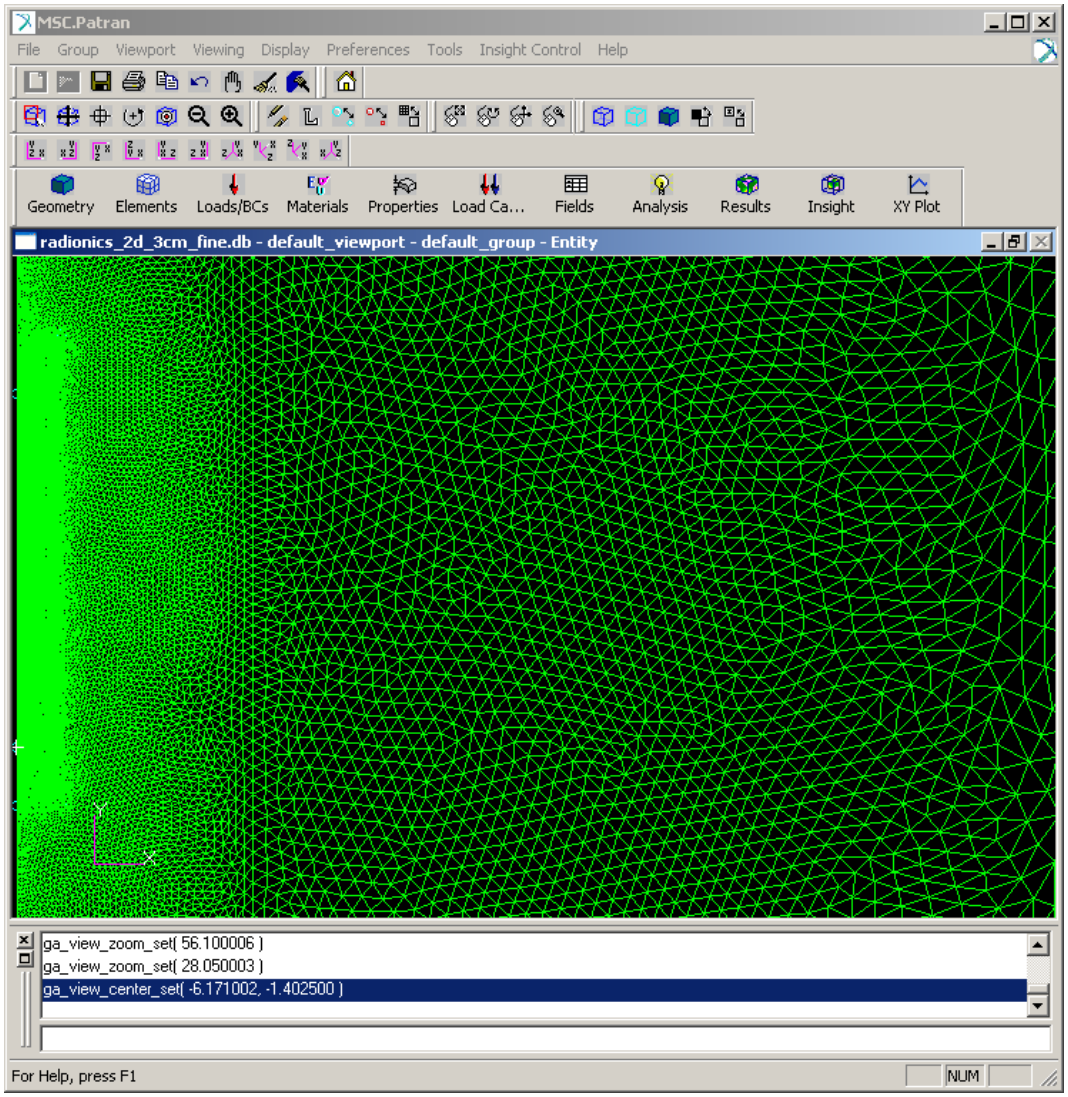

Figure 4.4: Generated Finite Element mesh. You can see the difference in density from the applicator to the edges of the model.

- Cooling: We simulated the cooling of the applicator with a constant temperature of 25°C along the electrode.

This concludes the preparation of the model. The next step is to export the model from Patran to Abaqus.

4.4.2 Solving in Abaqus 6.5-1

Porting the Patran output to Abaqus

The first step is to convert the output of Patran into a format suitable for this simulation scenario. Since Patran is not able to create an input file usable for a coupled thermal-electrical simulation. The procedure how to define the type of simulation (e.g. static stress analysis or steady state transport analysis) and, for that matter, the used equations, is based on [16]. To obtain a model definition suitable for my purpose I have to make the following changes to the file created by Patran:

First I need to change the element type to a type which supports electrical boundary conditions. This is done by adding an "E" to the element type definition. Since not every element type supports electrical boundary conditions we have to check with the documentation if the desired element type is available.

```
*ELEMENT, TYPE=DCAX3, ELSET=<NAME OF ELEMENT SET>
```

with

```
*ELEMENT, TYPE=DCAX3E, ELSET=<NAME OF ELEMENT SET>
```

This has to be done for each definition of an element set (the easiest way to find the required lines in the text file is to grep for "ELSET").

After changing the element types I have to set the correct analysis type. To do that I have to replace:

```
** Step 1, Default Static Step
** LoadCase, Default
**
*STEP, AMPLITUDE=RAMP, PERTURBATION
Linear Static Analysis
**
```

```
This load case is the default load case that always appears
**
*STATIC
```

with

```
*COUPLED THERMAL-ELECTRICAL, DELTMX=5.0, END=PERIOD
         0.05,          720., 1e-6, 30.
**
```

Table 4.2 describes the parameters used to define the simulation duration and the time increments which are to be used in this case.

DELTMX=5.0	This enables the automatic time incrementation in transient analysis. The numerical value prescribes the maximum temperature change in one time step
END=PERIOD	This is used to only analyze a prescribed time span
0.05	Initially allowed time increment (in seconds)
720	The duration (in seconds) for which the model has to be solved
1e-6	Minimum allowed time increment (in seconds)
30	Maximum allowed time increment (in seconds)

Table 4.2: Simulation parameters

The next step is to enter the actual material properties. The following code block shows how material properties are defined in Abaqus syntax:

```
**
*MATERIAL, NAME=LIV_MAT
**
*DENSITY
      0.00106,
**
```

```
*ELECTRICAL CONDUCTIVITY
       3.33E-4,
**
*CONDUCTIVITY, TYPE=ISO
       5.12E-4,
**
*SPECIFIC HEAT
          3.6,
```

Since I need to consider the effect of blood perfusion into my result I will have to define a subroutine which will calculate the energy loss due to perfusion (see 4.4.2 on how to create user routines). I need to tell Abaqus to use a user defined routine on a specific element set (in my case the set that describes the liver). This is done by introducing the following code:

```
**
*DFLUX, OP=NEW
LIVER, BFNU,          1.
**
```

The input file for the solver is now complete, and only the Fortran file with the user defined routines is missing.

Creating the Fortran routines for additional calculations and executing the model

I need user defined routines for two important parts in our simulation.

First I need to use the routine "*DFLUX*" to define the energy loss due to blood perfusion.

Secondly I need to control the applied energy to obtain temperatures between $\approx 95°C$ and $\approx 105°C$. I need to utilize the routines "*USDFLD*" and "*DISP*". In "*USDFLD*" I have to retrieve the current temperature of a node close to the applicator tip and store it as a variable. This value is accessed from the "*DISP*" routine which calculates the applied energy in a way that the maximum temperature can't exceed $105°C$.

You can find the complete source of the Fortran file in Appendix C.

After the Abaqus model file and the file for the user routines are prepared, the analysis can be started with the following command:

abaqus job=<ABAQUS INPUT FILE> user=<FILE WITH USERROUTINES>

4.4.3 Post-Processing

Visualize Data

After the simulation is done, I need to analyze the result. The first step is to check the plausibility of the result. For example I expected a final temperature of $\approx 95°C - \approx 105°C$ close to the applicator zone and a temperature of $\approx 37°C$ on the edge of the model. If the temperatures would be far of, it would probably safe to assume that an error happened in the Pre-Processing step. For my scenario the property to validate is as aforementioned the nodal temperature. Figure 5.1 on page 42 shows the temperature profile after a simulation of a 12 minutes radiofrequency application. In Abaqus you have various possibilities for visualizing your data. You can also create various overlays to compare results at different times (especially useful to analyze stress displacements) or you can create revolutions of any degree along the y axis of an axi-symmetric model to gain a better overview about the result in 3D (Figure 4.5 a 3D visualization of a 3D model).

Prepare Data for Export

The visualization and analysis features of any Post-Processor seldom provide the flexibility needed to perform advanced analysis of the obtained data. In this case it is necessary to be able to export either the whole result or just a subset of it in a format usable by other software such as Mathworks Matlab or Microsoft Excel. In Abaqus this is a relatively complex process, since it is not possible to simply export the result into a table format. I decided to select a row of radially distributed sample nodes and export it into a table which connects each nodal number to the corresponding temperature. The drawback was, that after the export, the nodes were missing their coordinate information, so I had to implement a simple spreadsheet in Excel which used the coordinate information from the Abaqus input file to correlate the nodal number with it's respective location information. This was done for several time-steps and thus allowed me to do an extensive analysis of the heating pattern at those time-steps.

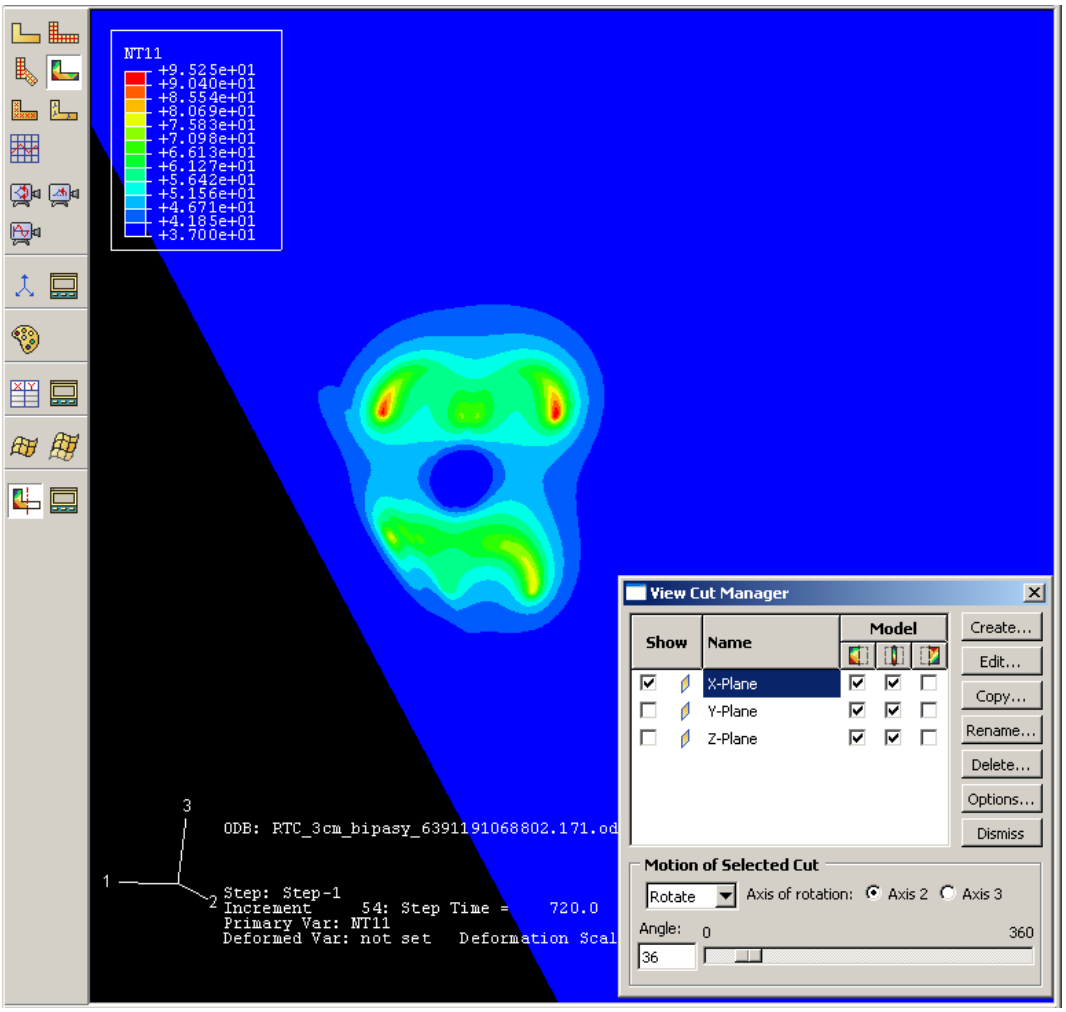

Figure 4.5: Screenshot of a 3D visualization with activated plane cut

Chapter 5

Relative Contribution of Thermal Conduction and Direct Heating During Tumor Ablation

5.1 Summary

Both radiofrequency (RF) and microwave (MW) ablation devices are clinically used for tumor ablation. Several studies report less dependence on vascular mediated cooling of MW compared to RF ablation. We created computer models of a cooled RF needle electrode, and a dipole MW antenna to determine differences in tissue heat transfer.

We created Finite Element computer models of a RF electrode (Cooled needle, 17 gauge), and a MW antenna (Dipole, 13 gauge). We simulated RF ablation for 12 min with power controlled to keep maximum tissue temperature at $100°C$, and MW ablation for 6 min with 75 W of power applied. For both models we considered change in electric and thermal tissue properties as well as perfusion depending on tissue temperature. We determined tissue temperature profile at the end of the ablation procedure and calculated effect of perfusion on both RF and MW ablation.

Maximum tissue temperature was $100°C$ for RF ablation, and $177°C$ for MW ablation. Lesion shape was ellipsoid for RF, and tear-drop shaped for MW ablation. MW ablation is less affected by tissue perfusion mainly due to the shorter ablation time and higher tissue temperature, but not due to MW providing deeper heating than RF. Both MW and RF applicators only produce significant direct heating within mm of the applicator, with most of the ablation zone created by thermal conduction.

Both RF and MW applicators only directly heat tissue in close proximity of the applicators. MW ablation allows for higher tissue temperatures than RF since MW propagation is not limited by tissue desiccation and charring. Higher temperatures coupled with lower treatment times result in reduced effects of perfusion on MW ablation

5.2 Introduction

Radiofrequency (RFA) and Microwave ablation (MWA) are used to destroy pathologic tissue by inducing tissue necrosis via heating of the targeted tissue. While ablation used for different diseases, here we consider tumor ablation, i.e. treatment of cancer. For tumor ablation, RFA is currently the most common thermal ablation therapy used in a clinical setting. Cryoablation, which is another fairly common tumor ablation modality, uses freezing instead of heat to kill tissue [11]. While surgical resection remains the therapy of choice for liver cancer, few patients have tumors suitable for surgical removal. Current studies suggest that RFA increases the patients 5 year survival rate and performs much better than chemotherapy alone [11, 8]. Radiofrequency ablation and Microwave ablation are clinically used for minimally invasive treatment of inoperable tumors of liver, as well as other organs such as lung, kidney and bone [13]. The most prevalent difference between RF and MW ablation are much higher tissue temperatures obtained with MW with typically shorter application times [40]. Highest temperatures of up to $\approx 100°C$ for RFA, and up to $\approx 160°C$ for MWA are obtained close to the applicator but temperature drops rapidly with distance from the applicator [15, 45]; the high thermal gradients result in considerable thermal conduction. Knowledge of regions where direct heating and thermal conduction are dominant is especially important when regions close to large vasculature are heated, where thermal conduction alone may not be sufficient to create temperatures in the therapeutic range ($> 50°C$) [14, 33]. In this study we examined the heating of liver tissue and determined the tissue regions where direct heating and where thermal conduction is dominating for the simulated RF and MW ablation devices. Since our models are designed to include common properties of ablation devices currently used in clinical practice, the clinical relevance of our results is likely, but has to be evaluated in further studies. We simulated RF and MW ablation using finite element method computer models, similar to previous studies [21, 24, 31, 47].

5.3 Methodology

We employed Finite Element Modeling and Finite Element Analysis to create and solve our experimental setup. We used Abaqus 6.5 for solving the RF model, FEMLab for the MW model, and Matlab 7.0 for further analysis of the generated results. The analysis was performed on a PC with 2GB RAM and a 3.2 GHz Intel Pentium 4 CPU. Both models were designed axi-symmetric due to the symmetry of electrode and antenna. Initial tissue temperature was 37°C, and this temperature was also applied to the model boundaries. For the model including perfusion according to Pennes' Bioheat Equation we assumed perfusion to stop when tissue coagulation occurs above $\approx 50°C$.

5.3.1 RF-Model (RFM):

We simulated a cooled needle electrode currently in use clinically (Cool-Tip, Valleylab, Boulder, CO). While there are other multi-tined electrodes used clinically, the simple geometry of the needle electrode allowed direct comparison to the MW antenna. The diameter of the exposed electrode is 1.5 mm and the length is 3 cm. This electrode uses internal cooling by circulating water which was simulated by applying 25°C as boundary condition on the electrode surface. In the clinical system applied power is controlled by tissue impedance with maximum tissue temperatures of $\approx 100°C$. In the computer model we controlled applied voltage such that maximum tissue temperature was 100°C during the 12 minutes ablation, since above 100°C tissue vaporization and charring limit further RF energy deposition.

5.3.2 RFM Tissue properties:

The tissue properties for the RF-Ablation Model (see table 5.1) were chosen according to [25], thus this simulation results are to be interpreted for a hepatic environment.

5.3.3 Microwave-Model (MWM):

We simulated a dipole antenna (2.3 mm diameter, 10 mm dipole length) (5.3.3) similar to antennas used clinically [38, 11]. While there are different antenna designs currently used in practice and in research, we chose to employ a dipole antenna due to the fact that this design is well documented and widely used

[38]. The antenna was inserted 90 mm into the tissue. 75 W of power was applied for 6 minutes at a frequency of 2.45 GHz. The SAR (specific absorption rate) is significantly affected by changing dielectric tissue properties as tissue water evaporates. Therefore in the electromagnetic (EM) model, tissue water related phenomena, including evaporation, diffusion and condensation, are simulated. The thermal model is based on expanded Bioheat equation which includes tissue water evaporation at higher temperature. Tissue properties are adjusted depending on changes in water content. This model generates results significant closer to experimental results than previous static antenna EM models and basic thermal models.

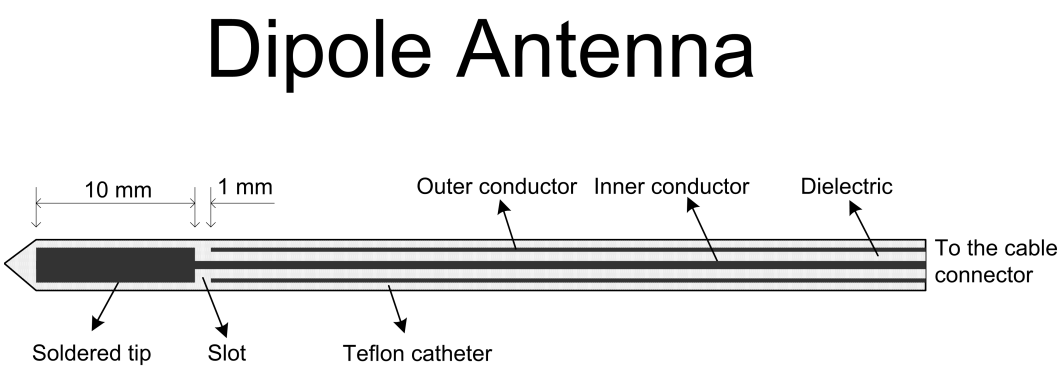

5.3.4 MWM Tissue properties:

In contrast to the RFM, c (specific heat) and ρ (tissue density) is calculated during the simulation by the following equations [46]:

Density:

$$\rho = v_w \times 1000 + 0.222 \times 1300 \tag{5.1}$$

v_W is the tissue water volume per unit volume of tissue, $0 \leq v_W \leq 0.778$. It is unit less. For normal tissue, $v_W = 0.778$. Proteins account for 22.2% of the total volume. Density of solid material is $1300 kg/m^3$ Density of water is $1000 kg/m^3$.

Specific Heat:

$$C = \sum_n w_n C_n \tag{5.2}$$

For liver tissue, we assume that tissue is composed by water and proteins. The equation for normal and desiccated liver tissue could be expressed as:

$$C = 4200 \times w_w + 1560 \times 0.27 \tag{5.3}$$

where C is the heat capacity $[J/g \bullet C]$, w_W is the remained tissue water mass per unit mass of tissue, $0 \leq w_W \leq 0.73$. The equation is based on that heat capacity of solid tissue materials (proteins) is $1560 J/g \bullet C$ and heat capacity of water is $4200 J/g \bullet C$.

Bioheat Equation[44]

$$\rho c \frac{\partial T}{\partial t} = \nabla \cdot k \nabla T + Q_A - Q_p \tag{5.4}$$

- ρ denotes the tissue density.
- c denotes the specific heat of the tissue.

Energy $Q_A(W/m^3)$ is applied to the tissue by the applicator (electrode or antenna), resulting in heating of the tissue. Some energy Q_p is carried away by blood perfusion.

$$Q_p = \rho_{bl} c_{bl} w_{bl} (T - T_{bl}) \tag{5.5}$$

Where $\rho_{bl}[kg/m^3], c_{bl}[J/kg \cdot K]$ and T_{bl} are density, specific heat and temperature of the blood, respectively. $T$is the tissue temperature, and w_{bl} is the blood perfusion (l/s)

To evaluate the relation between RFA and MWA we integrated each term over time. Please note, that even tough the terms are not independent from each other (e.g. perfusion / conduction) we could determine the relationship between those terms; since we modeled RFA and MWA with and without perfusion, we could directly observe how perfusion and thermal conduction are interrelated.

The temperature increase due to thermal conduction was calculated using the following equation:

$$\Delta T_{cond} = \int_t \frac{\nabla \cdot k \nabla T}{\rho c} \delta_t \tag{5.6}$$

In the same way, we determined temperature increase due to direct heating ($SAR(W/kg^3)$):

$$SAR = \frac{Q_A}{\rho} \tag{5.7}$$

$$\Delta T_{SAR} = \int_t \frac{SAR}{\rho c} \delta_t \tag{5.8}$$

and perfusion:

$$\Delta T_{Q_p} = \int_t \frac{Q_p}{\rho c} \delta_t \tag{5.9}$$

$\Delta T_{cond}, \Delta T_{SAR}, \Delta T_{Q_p}$ were calculated for the 12 minutes RFM simulation, the 6 minutes MWM simulation. We also determined $\Delta T_{cond}, \Delta T_{SAR}, \Delta T_{Q_p}$ for the 0 minutes - 6 minutes and 6 minutes - 12 minutes time spans for the RFM simulation; for the 0 minutes - 3 minutes and 3 minutes - 6 minutes for the MWM simulation. This was done to determine the relative contribution $\Delta T_{cond}, \Delta T_{SAR}, \Delta T_{Q_p}$ in relation to different time spans. The sum of the three terms in 5.6 5.8 5.9 equates to the total tissue temperature rise:

$$\Delta T = \Delta T_{cond} + \Delta T_{SAR} + \Delta T_{Q_p} \tag{5.10}$$

and the final tissue temperature is:

$$T = 37°C + \Delta T \tag{5.11}$$

5.3.5 Coagulation Zone Boundary:

Even though tissue damage depends both on temperature and time [10], we found in previous studies that the 50 °C isotherm correlates with coagulation zone boundary within acceptable accuracy [24]. Therefore we used the 50 °C isotherm to determine ablation zone boundaries.

5.4 Results

Maximum temperatures were $\approx 100°C$ in the RF model, and 177°C in the MW model; tissue charring and tissue vapor does not limit propagation of microwaves, so a higher temperature can be achieved compared to RF. These temperature values are comparable to temperatures measured in vivo [15, 45].

ρ, kgm^3	1060
$c, J(kg * K)^-1$	3600
$k, W(m * K)^-1$	0.512
$\sigma, Sm^-1 at 50kHz$	0.333

Table 5.1: Hepatic tissue properties

The final coagulation zone diameters were 26 mm for the perfused RFM (Figure 5.1), and 36 mm for the unperfused RFM; diameters were 23 mm for the perfused MWM (Figure 5.2) and 26 mm for the unperfused MWM. For the 12 minutes RFM simulation with perfusion, thermal conduction dominates in the range from 12 to 19 mm radially (Figure 5.3). For the 6 minutes MWM simulation with perfusion, thermal conduction is dominating the range > 20 mm radially (Figure 5.4). If temperature loss due to blood perfusion is not simulated, direct heating is dominating throughout the RFM (Figure 5.5) and MWM (Figure 5.6). We also determined the time depended contribution of $\Delta T_{cond}, \Delta T_{SAR}, \Delta T_{Q_p}$. For the 0 minutes - 6 minutes time span in the RFM (Figure 5.7) direct heating was dominating the whole model, because the influence of blood perfusion has not yet ceased (temperatures $< 50°C$) . For the 0 minutes - 3 minutes MWM (Figure 5.8) time span we can see that thermal conduction dominates the range from 9 mm - 11 mm radially because temperatures $> 50°C$ are already reached in this area. For the 6 min - 12 min time span in the RFM (Figure 5.9) and the 3 minutes - 6 minutes time span in the MWM (Figure 5.10) the relative contribution of direct heating is dominating the whole model. We also determined the area and the contributed amount of direct heating to the increase of tissue temperature. Figure 5.11 shows the influence of direct heating in the RF ablation simulation compared to the influence of direct heating in the MW ablation simulation. At each radial location, the fraction of total power within that radius (i.e. integral between 0 and radius) is plotted. For RF, 90% of total power is deposited within 5 mm; for MW, 90% of total power is deposited within 6 mm.

5.5 Discussion

While it has been previously suggested that MWA performs better next to large vasculature due to a larger direct heating area, we found that the volumes of direct heating are similar between RFA and MWA (Figures 5.4, 5.7).

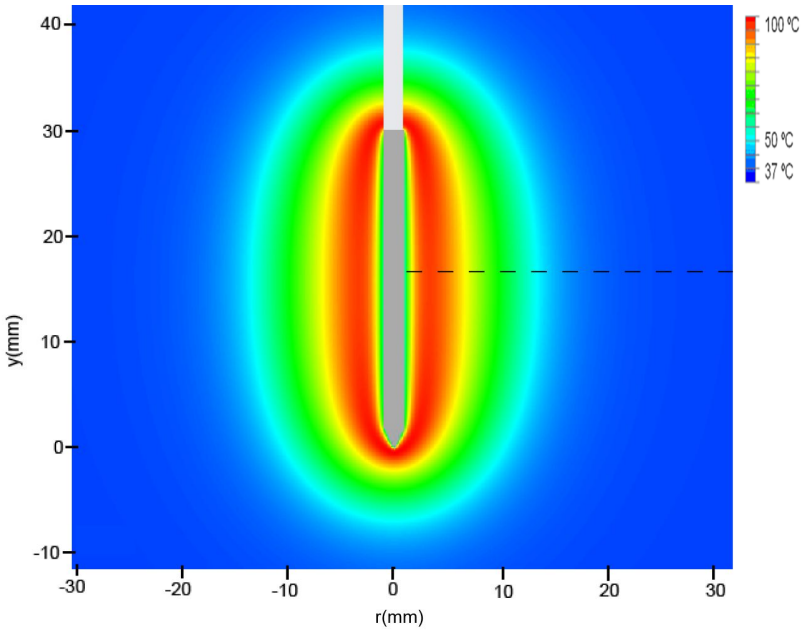

Figure 5.1: RF Temperature profile after 12 min - Temperature profile after 12 minutes of RF-Ablation. The dotted line shows the location where analysis was performed for Figure 5.4. The area with temperatures $> 50°C$ is the coagulation zone.

Our models suggest that the reason MWA is less affected by perfusion is likely that MW heating is not limited by tissue charring around the applicator. This results in higher temperatures during MWA (Figure 5.2). The resulting shorter application times make MWA less susceptible to perfusion effects as demonstrated by our models (Figure 5.7).

Shibata et. al [37] performed a study on the effects of in-vivo microwave and radiofrequency ablation in pig liver. Even though we were not able to compare the ablation zone diameters directly due to the different ablation times used in Shibata et al., we did observe the considerably higher ellipticity of the ablation zone shapes note there.

Initially direct heating is dominating everywhere for both RF and MW ablation since tissue temperature is uniform (i.e. no temperature gradient and no heat flux). The integrals of the different heating terms show that for MW ablation, direct heating due to dielectric losses is dominating up to a radius of 20 mm over the 6 minutes MW ablation. Further away thermal conduction and direct heating have similar contributions (Figure 5.4). For RF ablation thermal conduction is dominating in the range from 12 mm to 19 mm radially over the 12 minutes procedure while direct heating due to resistive losses is dominating elsewhere (Figure 5.3). The higher contribution of thermal conduc-

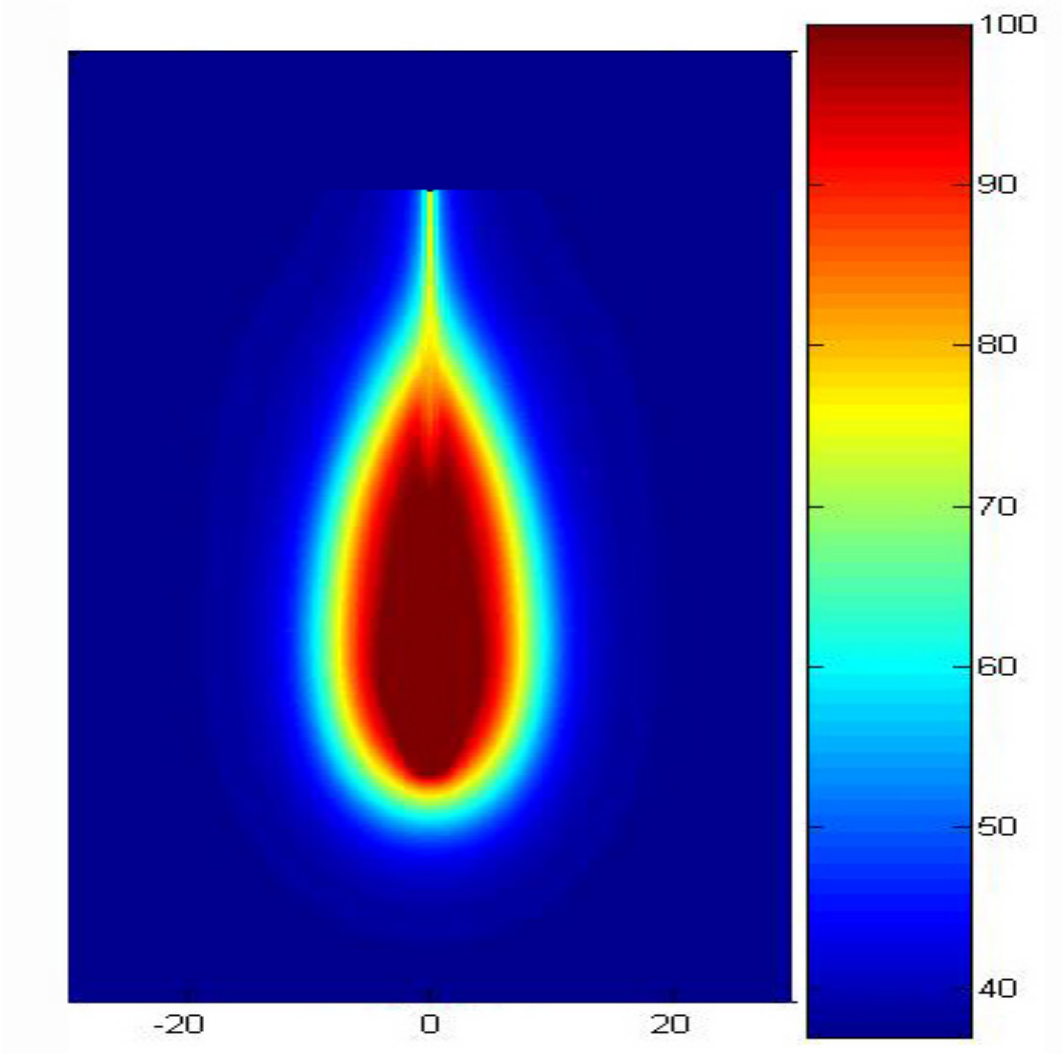

Figure 5.2: Temperature profile after 6 minutes of MW-Ablation. The dotted line shows the location where analysis was performed for Figure 5.4. The area with temperatures $> 50°C$ is the ablation zone.

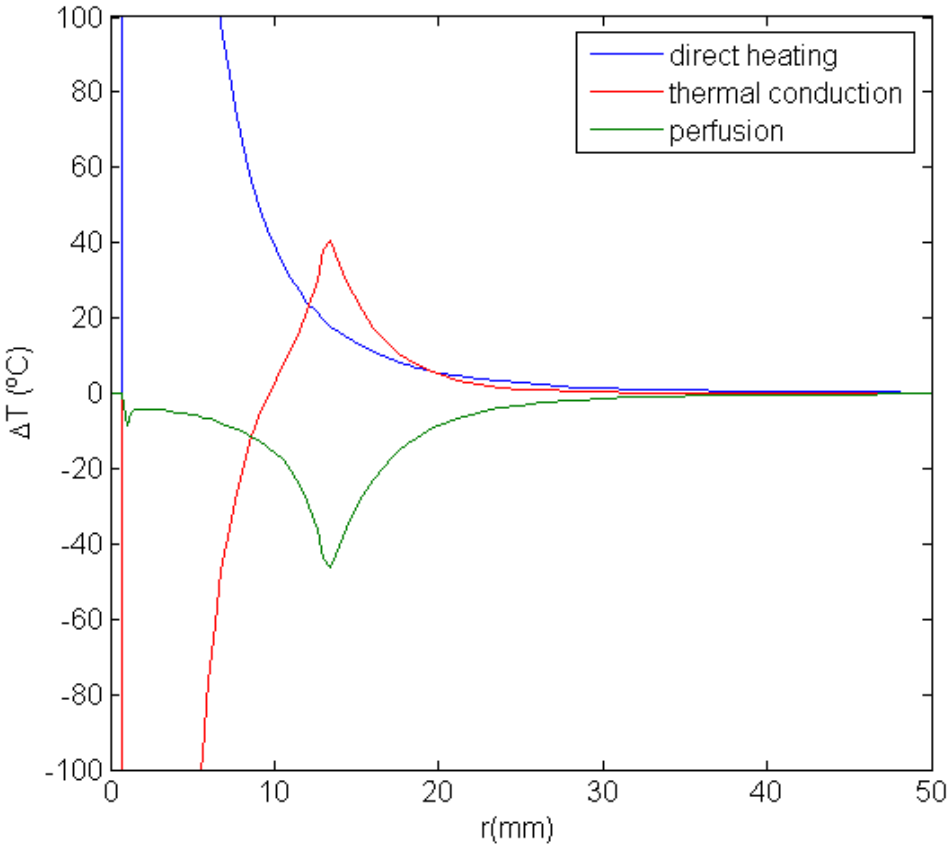

Figure 5.3: 12 minute RF-Ablation with perfusion -Temperature increase δT due to direct heating (blue), thermal conduction (red), and perfusion (green). Over the 12 minutes ablation procedure, thermal conduction dominates in the range from 12 to 19 mm radially.

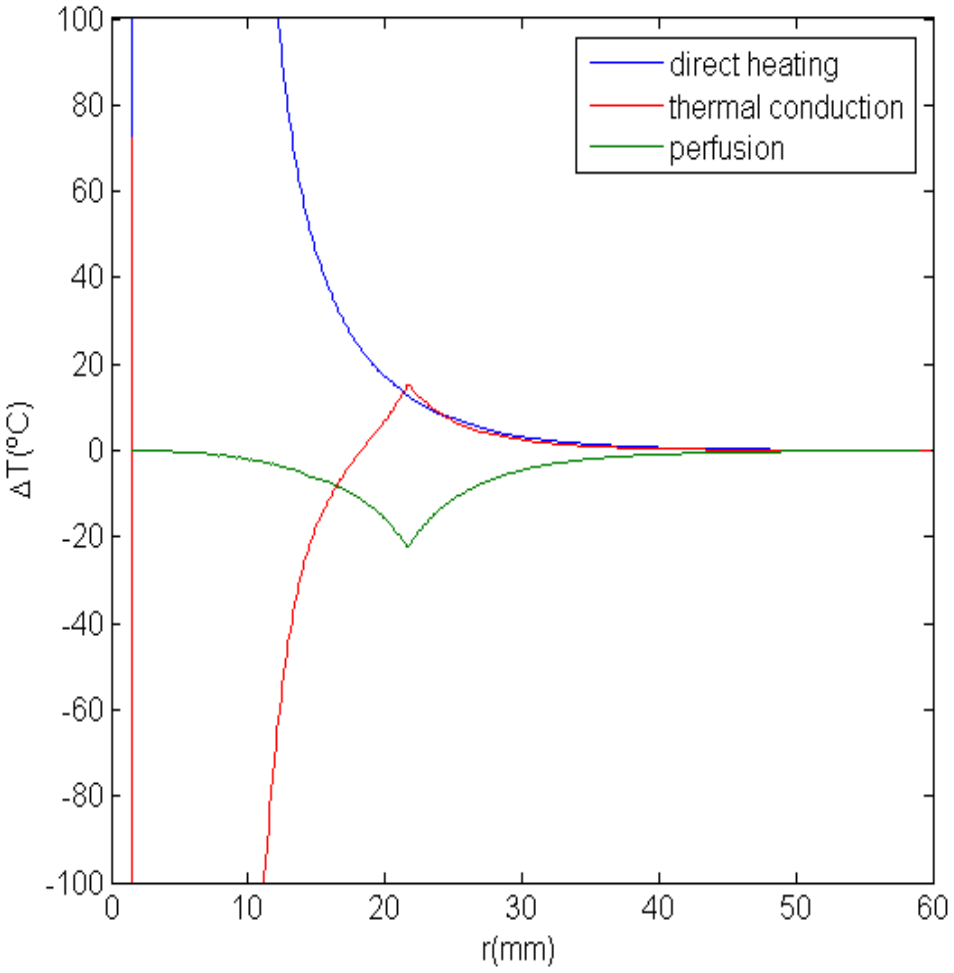

Figure 5.4: 6 minute MW-Ablation with perfusion - Temperature increase δT due to direct heating (blue), thermal conduction (red), and perfusion (green). Over the 6 min ablation procedure, direct heating is dominating the range up to 20 mm radially.

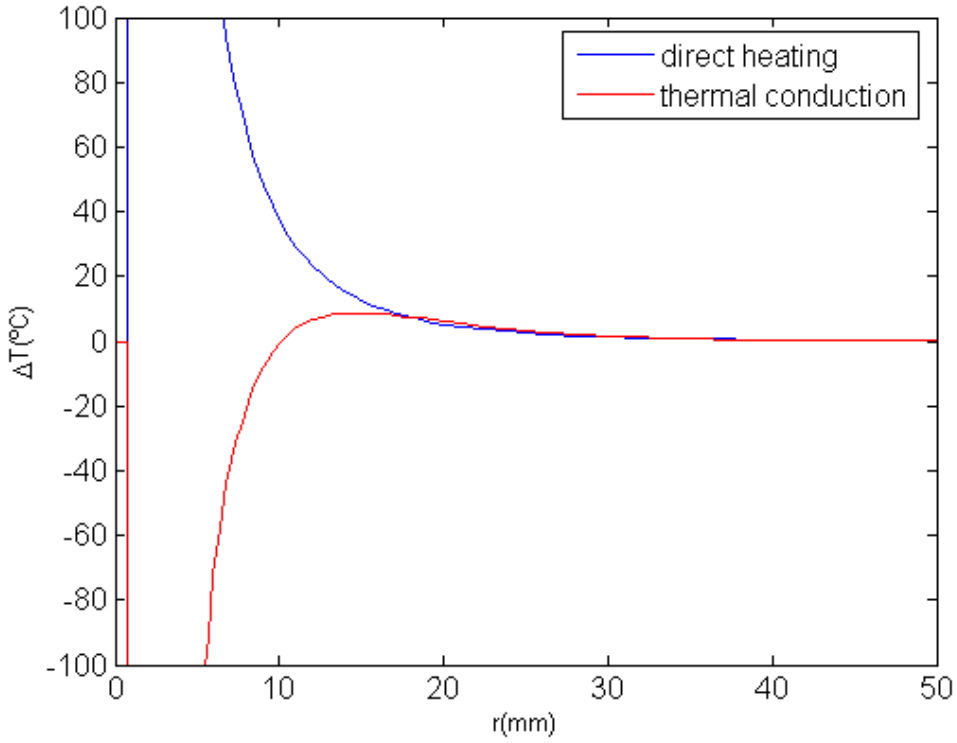

Figure 5.5: 12 minute RF-Ablation without perfusion - Temperature increase δT due to direct heating (blue), thermal conduction (red). Due to the absence of a high temperature gradient at the ablation zone boundary because blood perfusion was not included in this model, direct heating is dominating throughout the model.

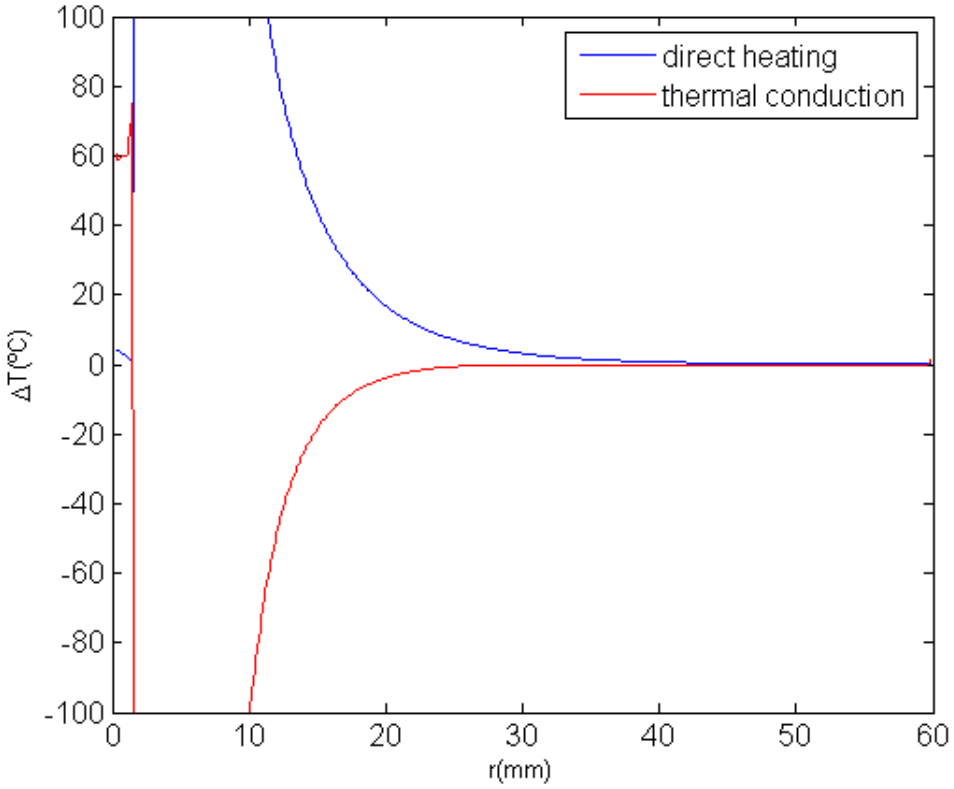

Figure 5.6: 6 minute MW-Ablation without perfusion - Temperature increase δT due to direct heating (blue), thermal conduction (red). Due to the absence of a high temperature gradient at the ablation zone boundary because blood perfusion was not included in this model, direct heating is dominating throughout the model.

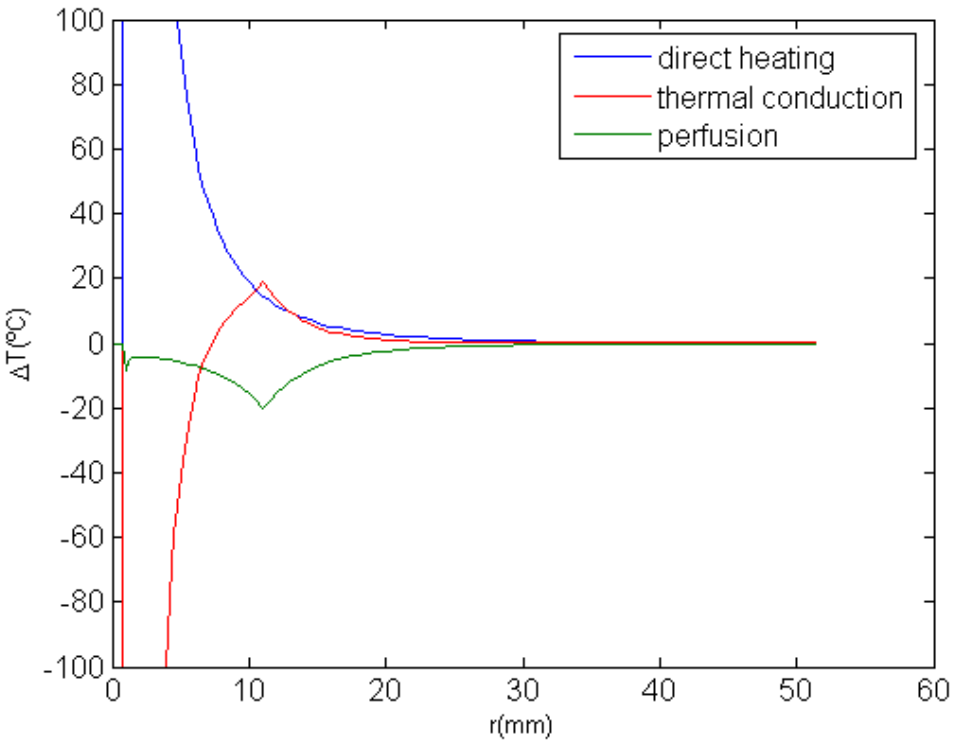

Figure 5.7: RF Ablation 0-6 Min with perfusion - Temperature increase δT due to direct heating (blue), thermal conduction (red), and perfusion (green). Over the first 6 minutes of the ablation procedure, thermal conduction dominates in the range from 9 mm to 11 mm radially.

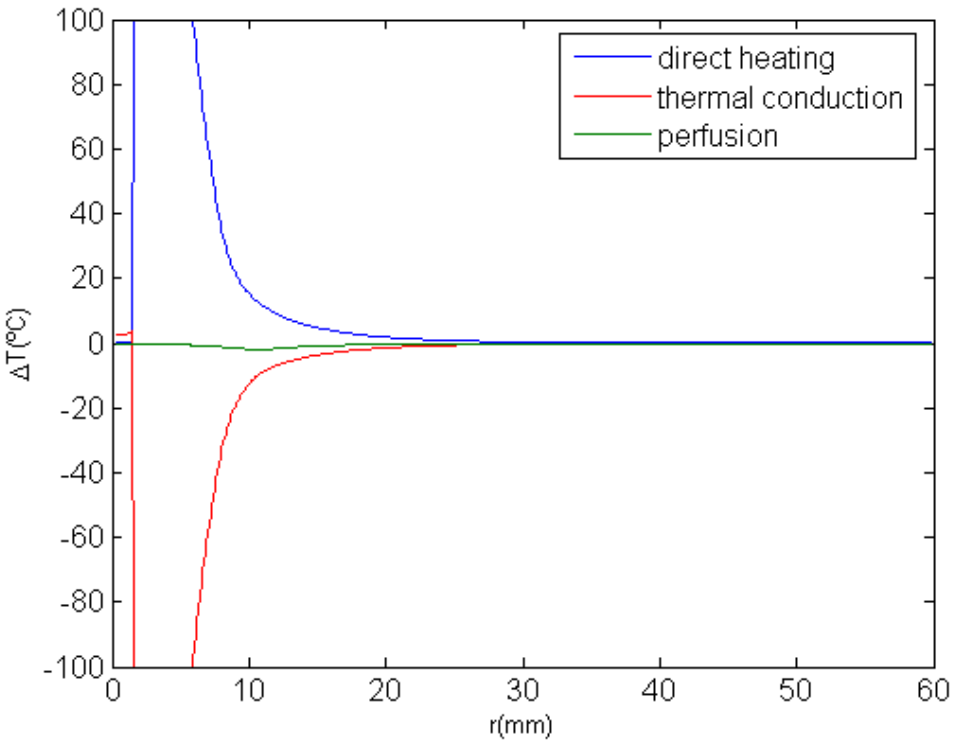

Figure 5.8: MW Ablation 0-3 Min with perfusion - Temperature increase δT due to direct heating (blue), thermal conduction (red), and perfusion (green). Over the first 3 minutes of the ablation procedure, direct heating is dominating everywhere.

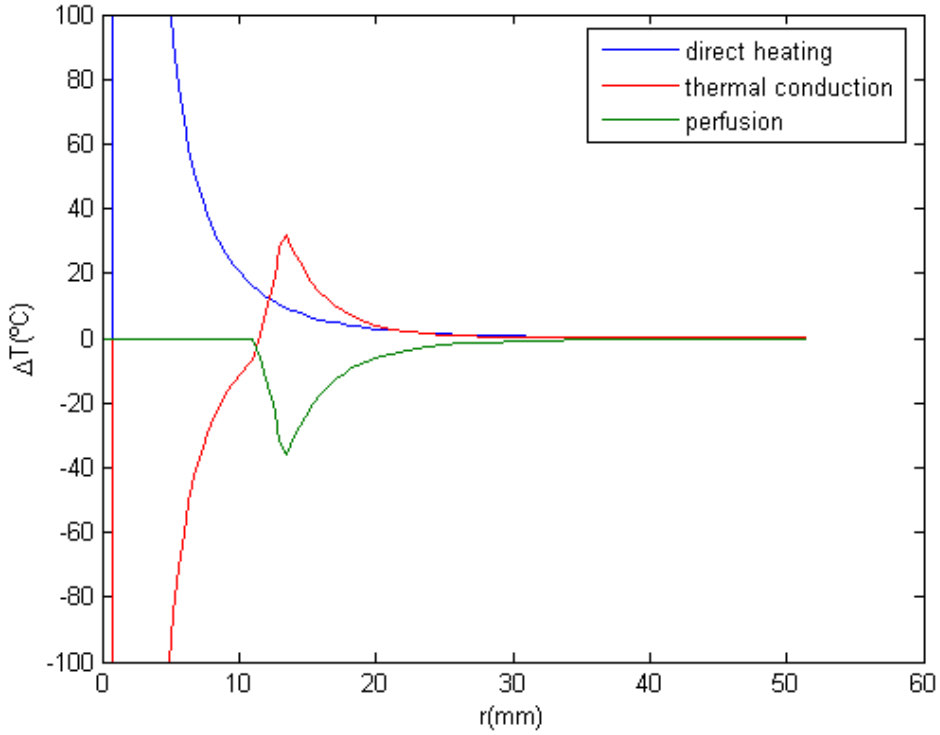

Figure 5.9: RF Ablation 6-12 Min with perfusion - Temperature increase δT due to direct heating (blue), thermal conduction (red), and perfusion (green). Over the last 6 minutes of the ablation procedure, thermal conduction dominates in the range from 12 mm to 20 mm radially.

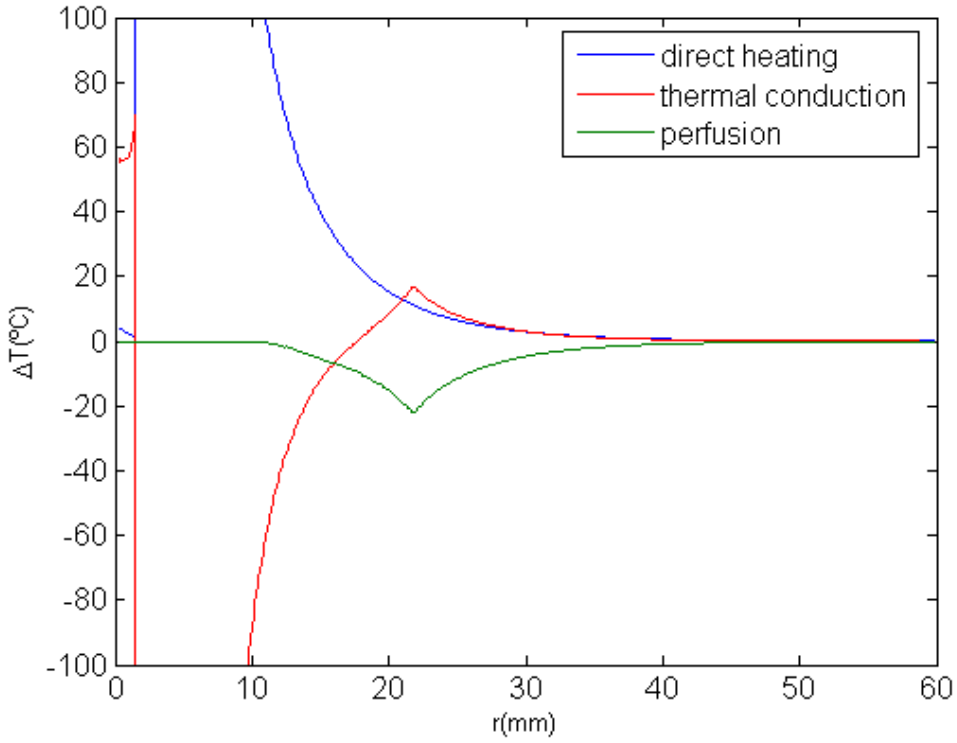

Figure 5.10: MW Ablation 3-6 Min with perfusion - Temperature increase δT due to direct heating (blue), thermal conduction (red), and perfusion (green). In the time between 3 minutes and 6 minutes of the ablation procedure, thermal conduction contributes significantly to tissue heating in the range from 20mm to 30mm radially.

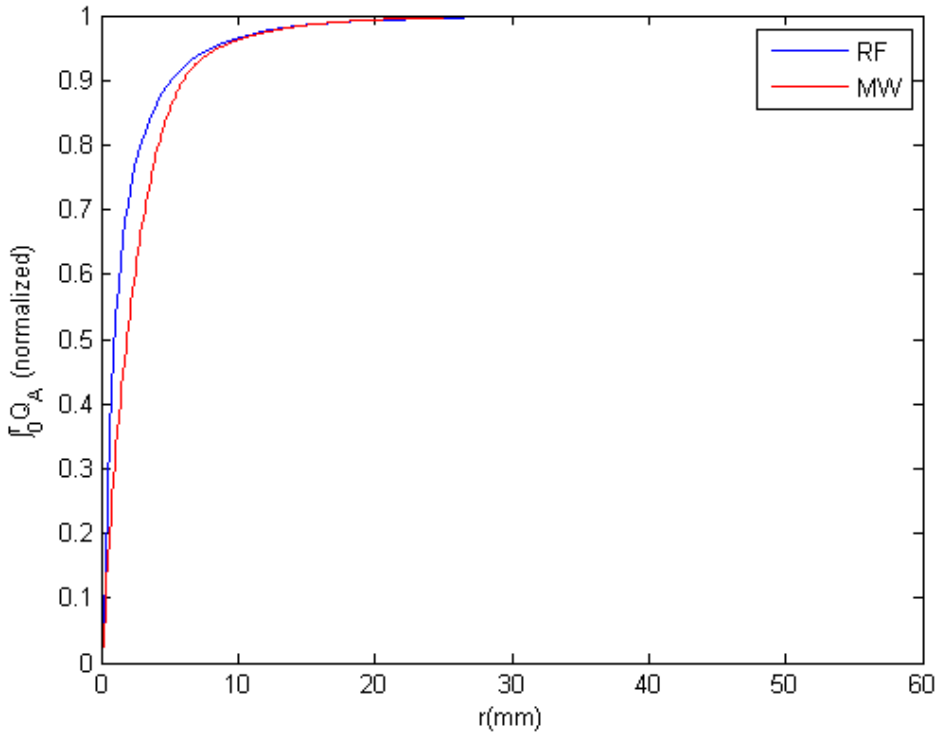

Figure 5.11: Comparison of the influence of direct heating during RF and MW ablation - Comparison of the influence of direct heating during RF and MW ablation. At each radial distance (r), the fraction of power deposited within that radius is shown. For RF, 90% of total power is deposited within 5 mm; for MW, 90% of total power is deposited within 6 mm.

tion near the 50°C-isotherm can be attributed to high temperature gradients occurring at the border of the perfusion zone (50°C). Tissue cooling due to perfusion is highest just below 50°C, and zero above 50°C; this discontinuity in perfusion promotes high thermal gradients, and increased thermal flux near the coagulation zone boundary. Since this discontinuity of thermal gradients is missing in the non-perfused models, the thermal conduction term is significantly smaller near the coagulation zone boundary (Figures 5.5, 5.6). Further notable is that thermal conduction contributes little during the first half of the RF and MW procedure (Figures 5.7, 5.8), with more significant contribution during the second half (Figures 5.9, 5.10). In fact, thermal conduction has similar contribution during both RF and MW ablation for the first 6 minutes (Figures 5.4, 5.7). Therefore, MWA may have clinical advantages close to large vasculature due to the shorter required treatment time compared to RFA.

5.6 Conclusions

During RF ablation tissue perfusion and thermal conduction contribute more towards tissue cooling and heating compared to MW ablation. This is mainly due to the longer session times necessary with RF ablation, as tissue temperatures are significantly lower compared to MW ablation. The reduced influence of thermal conduction and perfusion due to shorter session times may in part explain why in vivo studies, MW coagulation zones are less affected by tissue perfusion compared to RF [45]. The region of direct heating is not significantly different between MW and RF ablation.

Chapter 6

Conclusion

6.1 Summary

Finite Element Analysis is an important tool in today's sciences. It is used in almost every research area in today's life, ranging from automotive industries to applications in *Biomedical Engineering*. Simulation of complex systems helps us to develop and improve instruments without actually building a single thing and thus reduces the cost of instrument development. Another important aspect is - especially in the field of *Biomedical Engineering* - patient safety. Most medical instruments have to be extensively tested before they can be tried on animals or even humans. Finite Element Analysis allows to try out various parameters and develop an optimal solution. It furthers allows to gain insights into processes which are regularly used today, but are not fully understood.

6.2 Outlook

The next step to increase the overall radiofrequency ablation performance is in my opinion to create patient specific models. These models could be created from a patient's computer tomography. This personalized models could help the clinician to try out several treatment variations before the actual surgery.

Another hot topic in current academic research is the combination of heat based ablation with the use of special prepared chemotherapeutics. Viglianti et. al. published a study [41] about the use of thermally activated liposomes loaded with doxorubicin (a widely used multi purpose chemotherapeutics). The idea behind this approach is to deliver the liposomes to the ablation zone where high temperatures ($> 40°C$) "crack up" the liposomes and release the

chemotherapeutic agent. The main goal of this approach is to deliver the toxic agent directly to the tumor site without being active in the rest of the patient's system. This may improve the overall health condition of a patient during the course of a chemotherapy. Another positive effect is the potential increase of the coagulation volume because of the agent's activity in temperature regions where tissue necrosis is not achievable (temperatures $> 40°C and < 50°C$).

List of Tables

2.1 Frequency of use of different ablation modalities in clinical applications [43]. 4

3.1 Summary of features differentiating benign and malignant neoplasms 16

4.1 Hepatic tissue properties 28
4.2 Simulation parameters 31

5.1 Hepatic tissue properties 41

Appendix A

Bibliography

[1] *Abaqus 6.5 Manual*. 2005.

[2] M. Ahmed, S. Melvyn Lobo, J. Weinstein, J. B Kruskal, G. S. Gazelle, E. F Halpern, S. Karim Afzal, Robert E Lenkinski, and S. Nahum Goldberg. Improved coagulation with saline solution pretreatment during radiofrequency tumor ablation in a canine model. *J Vasc Interv Radiol*, 13(7):717–724, Jul 2002.

[3] M. Ahmed, A. N Lukyanov, V. Torchilin, H. Tournier, A. N Schneider, and S. Nahum Goldberg. Combined radiofrequency ablation and adjuvant liposomal chemotherapy: effect of chemotherapeutic agent, nanoparticle size, and circulation time. *J Vasc Interv Radiol*, 16(10):1365–1371, Oct 2005.

[4] M. Ahmed, J. Weinstein, Z. Liu, K. S Afzal, Cl. Horkan, J. B Kruskal, and S. Nahum Goldberg. Image-guided percutaneous chemical and radiofrequency tumor ablation in an animal model. *J Vasc Interv Radiol*, 14(8):1045–1052, Aug 2003.

[5] A. M. Di Bisceglie, V. K. Rustgi, J. H. Hoofnagle, G. M. Dusheiko, and M. T. Lotze. Nih conference. hepatocellular carcinoma. *Ann Intern Med*, 108(3):390–401, Mar 1988.

[6] G. H Bourne. *An introduction to functional histology*. Little, Brown, 1953.

[7] P. Chandrasoma and C. R. Taylor. *Concise Pathology*. McGraw-Hill Publishing Co, 1997.

[8] B. Decadt and A. K Siriwardena. Radiofrequency ablation of liver tumours: systematic review. *Lancet Oncol*, 5(9):550–560, Sep 2004.

[9] V. T. Devita, S. Hellman, and S. A. Rosenberg. *Cancer: Principles And Practice Of Oncology*. Lippincott Williams & Wilkins, 2004.

[10] M. W. Dewhirst, B. L. Viglianti, M. Lora-Michiels, M. Hanson, and P. J. Hoopes. Basic principles of thermal dosimetry and thermal thresholds for

tissue damage from hyperthermia. *Int J Hyperthermia*, 19(3):267–294, 2003.

[11] G. D. Dodd, M. C. Soulen, R. A. Kane, T. Livraghi, W. R. Lees, Y. Yamashita, A. R. Gillams, O. I. Karahan, and H. Rhim. Minimally invasive treatment of malignant hepatic tumors: at the threshold of a major breakthrough. *Radiographics*, 20(1):9–27, 2000.

[12] W. F. Ganong. *Review of Medical Physiology*. McGraw-Hill Publishing Co., 2005.

[13] A. R. Gillams. The use of radiofrequency in cancer. *Br J Cancer*, 92(10):1825–1829, May 2005.

[14] S. N. Goldberg, G. S. Gazelle, and P. R. Mueller. Thermal ablation therapy for focal malignancy: a unified approach to underlying principles, techniques, and diagnostic imaging guidance. *AJR Am J Roentgenol*, 174(2):323–331, Feb 2000.

[15] S. N. Goldberg, G. S. Gazelle, L. Solbiati, W. J. Rittman, and P. R. Mueller. Radiofrequency tissue ablation: increased lesion diameter with a perfusion electrode. *Acad Radiol*, 3(8):636–644, Aug 1996.

[16] D. Haemmerich. *Finite Element Modeling of Hepatic Radiofrequency Ablation*. PhD thesis, University of Wisconsin - Madison, 2001.

[17] D. Haemmerich, L. Chachati, A. S Wright, D. M Mahvi, F. T Lee, and J. G Webster. Hepatic radiofrequency ablation with internally cooled probes: effect of coolant temperature on lesion size. *IEEE Trans Biomed Eng*, 50(4):493–500, Apr 2003.

[18] D. Haemmerich and P. F. Laeseke. Thermal tumour ablation: devices, clinical applications and future directions. *Int J Hyperthermia*, 21(8):755–760, Dec 2005.

[19] D. Haemmerich, R. Ozkan, S. Tungjitkusolmun, J. Z. Tsai, D. M. Mahvi, S. T. Staelin, and J. G. Webster. Changes in electrical resistivity of swine liver after occlusion and postmortem. *Med Biol Eng Comput*, 40(1):29–33, Jan 2002.

[20] D. Haemmerich, S. T. Staelin, J. Z. Tsai, S. Tungjitkusolmun, D. M. Mahvi, and J. G. Webster. In vivo electrical conductivity of hepatic tumours. *Physiol Meas*, 24(2):251–260, May 2003.

[21] D. Haemmerich, S. T. Staelin, S. Tungjitkusolmun, F. T. Lee, D. M. Mahvi, and J. G. Webster. Hepatic bipolar radio-frequency ablation between separated multiprong electrodes. *IEEE Trans Biomed Eng*, 48(10):1145–1152, Oct 2001.

[22] D. Haemmerich, S. Tungjitkusolmun, S. Tyler Staelin, F. T Lee, D. M Mahvi, and J. G Webster. Finite-element analysis of hepatic multiple probe radio-frequency ablation. *IEEE Trans Biomed Eng*, 49(8):836–842, Aug 2002.

[23] D. Haemmerich and J. G Webster. Automatic control of finite element models for temperature-controlled radiofrequency ablation. *Biomed Eng Online*, 4(1):42, 2005.

[24] D. Haemmerich, JG. Webster, and DM. Mahvi. Thermal dose versus isotherm as lesion boundary estimator for cardiac and hepatic radiofrequency ablation. In *IEEE Engineering in Medicine and Biology Conference*, 2003.

[25] D. Haemmerich, A. W. Wright, D. M. Mahvi, F. T. Lee, and J. G. Webster. Hepatic bipolar radiofrequency ablation creates coagulation zones close to blood vessels: a finite element study. *Med Biol Eng Comput*, 41(3):317–323, May 2003.

[26] T. R. Harrison, D.s L. Kasper, E. Braunwald, and A. S. Fauci. *Harrison's Principles of Internal Medicine.* McGraw-Hill Education, 2004.

[27] L. C. Junqueira and J. Carneiro. *Basic Histology : Text & Atlas (Basic Histology).* McGraw-Hill Medical, 2005.

[28] B. G. Katzung. *Basic & Clinical Pharmacology (LANGE Basic Science).* McGraw-Hill Medical, 2003.

[29] R. W. Lewis, P. Nithiarasu, and K. N. Seetharamu. *Fundamentals of the Finite Element Method for Heat and Fluid Flow.* John Wiley and Sons Ltd, 2004.

[30] G. R. Liu and S. Quek. *Finite Element Method. A Practical Course.* Elsevier LTD, Oxford, 2003.

[31] S. M. Lobo, Z-J. Liu, N. C. Yu, S. Humphries, M. Ahmed, E. R. Cosman, R. E. Lenkinski, W. Goldberg, and S. N. Goldberg. Rf tumour ablation: computer simulation and mathematical modelling of the effects of electrical and thermal conductivity. *Int J Hyperthermia*, 21(3):199–213, May 2005.

[32] S. Melvyn Lobo, K. S Afzal, M. Ahmed, J. B Kruskal, R. E Lenkinski, and S. Nahum Goldberg. Radiofrequency ablation: modeling the enhanced temperature response to adjuvant nacl pretreatment. *Radiology*, 230(1):175–182, Jan 2004.

[33] D. Panescu, J. G. Whayne, S. D. Fleischman, M. S. Mirotznik, D. K. Swanson, and J. G. Webster. Three-dimensional finite element analysis of current density and temperature distributions during radio-frequency ablation. *IEEE Trans Biomed Eng*, 42(9):879–890, Sep 1995.

[34] S. L. Parker, T. Tong, S. Bolden, and P. A. Wingo. Cancer statistics, 1996. *CA Cancer J Clin*, 46(1):5–27, 1996.

[35] P. L Pereira, J. Trübenbach, M. Schenk, J. Subke, S. Kroeber, I. Schaefer, C. T Remy, D. Schmidt, J. Brieger, and C. D Claussen. Radiofrequency ablation: in vivo comparison of four commercially available devices in pig livers. *Radiology*, 232(2):482–490, Aug 2004.

[36] W. Schramm, D. Yang, and D. Haemmerich. Contribution of direct heating, thermal conduction and perfusion during radiofrequency and microwave ablation. In *Engineering in Medicine and Biology Society, 2006. EMBS '06. 28th Annual International Conference of the IEEE*, pages 5013–5016, Aug. 2006.

[37] T. Shibata, T. Niinobu, and N. Ogata. Comparison of the effects of in-vivo thermal ablation of pig liver by microwave and radiofrequency coagulation. *J Hepatobiliary Pancreat Surg*, 7(6):592–598, 2000.

[38] C. J Simon, D. E Dupuy, and W. W Mayo-Smith. Microwave ablation: principles and applications. *Radiographics*, 25 Suppl 1:S69–S83, Oct 2005.

[39] R. G. Simonetti, C. Cammà, F. Fiorello, F. Politi, G. D'Amico, and L. Pagliaro. Hepatocellular carcinoma. a worldwide problem and the major risk factors. *Dig Dis Sci*, 36(7):962–972, Jul 1991.

[40] A. D. Strickland, P. J. Clegg, N. J. Cronin, B. Swift, M. Festing, K. P. West, G. S M Robertson, and D. M. Lloyd. Experimental study of large-volume microwave ablation in the liver. *Br J Surg*, 89(8):1003–1007, Aug 2002.

[41] B. L Viglianti, S. A Abraham, C. R Michelich, P.l S Yarmolenko, J. R MacFall, M. B Bally, and M. W Dewhirst. In vivo monitoring of tissue pharmacokinetics of liposome/drug using MRI: illustration of targeted delivery. *Magn Reson Med*, 51(6):1153–1162, Jun 2004.

[42] L. W. Way and G. M. Doherty. *Current Surgical Diagnosis and Treatment (Current Surgical Diagnosis & Treatment)*. Appleton and Lange, 2002.

[43] J. G. Webster, editor. *Encyclopedia of Medical Devices and Instrumentation, 6 Volume Set, 2nd Edition, Chapter XX*. Wiley, 2006.

[44] E. H. Wissler. Pennes' 1948 paper revisited. *J Appl Physiol*, 85(1):35–41, Jul 1998.

[45] A. S Wright, L. A Sampson, T. F Warner, D. M Mahvi, and F. T Lee. Radiofrequency versus microwave ablation in a hepatic porcine model. *Radiology*, 236(1):132–139, Jul 2005.

[46] D. Yang. *Measurements, antenna design and advanced computer modeling for microwwave tissue ablation*. PhD thesis, University of Wisconsin, 2006.

[47] D. Yang, J. M Bertram, M. C Converse, A. P O'Rourke, J. G Webster, S. C Hagness, J. A Will, and D. M Mahvi. A floating sleeve antenna yields localized hepatic microwave ablation. *IEEE Trans Biomed Eng*, 53(3):533–537, Mar 2006.

Appendix B

Sample Abaqus Input-File

```
*HEADING
ABAQUS job created on 24-Apr-06 at 13:43:07
**
** Defining the model nodes
*NODE
       1,            0.,           30.
       2,   5.55112E-17,            0.

       . . .
       . . .
       . . .

   18912,      0.514003,       50.2918
   18913,      0.208971,         50.27
**
**
** Defining the model elements
*ELEMENT, TYPE=DCAX3E, ELSET=LIVER
    5192,    2919,    2917,    2903
    5193,    2920,    3507,    2919

  .  . . .
  .  . . .
  .  . . .

   35579,   12554,   18868,   12555
   35580,   18867,   12555,   18868
**
** liver
**
*SOLID SECTION, ELSET=LIVER, MATERIAL=LIV_MAT
```

```
          1.,
**
** electrode
**
*SOLID SECTION, ELSET=ELECTRODE, MATERIAL=FE_MAT
          1.,
**
** stent
**
*SOLID SECTION, ELSET=STENT, MATERIAL=PU_MAT
          1.,
**
*MATERIAL, NAME=LIV_MAT
**
*USER DEFINED FIELD
** allocate four state-dependent variables
*DEPVAR
4
**
**USER OUTPUT VARIABLES
**1
**
*DENSITY
      0.00106,
**
*ELECTRICAL CONDUCTIVITY
       3.33E-4,
**
*CONDUCTIVITY, TYPE=ISO
       5.12E-4,
**
*SPECIFIC HEAT
          3.6,
**
** fe_mat
**
*MATERIAL, NAME=FE_MAT
**
*DENSITY
      6.45E-3,
**
*ELECTRICAL CONDUCTIVITY
1E5,
**
*CONDUCTIVITY, TYPE=ISO
       0.018,
```

```
**
*SPECIFIC HEAT
       0.84,
**
** pu_mat
** Date: 26-Jul-01           Time: 15:24:03
**
*MATERIAL, NAME=PU_MAT
**
*DENSITY
      7E-5,
**
*ELECTRICAL CONDUCTIVITY
1E-8,
**
*CONDUCTIVITY, TYPE=ISO
       2.6E-5,
**
*SPECIFIC HEAT
       1.045,
**
**
*INITIAL CONDITIONS, TYPE=FIELD, VARIABLE=5
INI_TMP, 0.
**INITIAL CONDITIONS, TYPE=FIELD, VARIABLE=2
**INI_TMP, 0.
**INITIAL CONDITIONS, TYPE=FIELD, VARIABLE=1
**INI_TMP, 0.
**
**
** ini_tmp
**
*INITIAL CONDITIONS, TYPE=TEMPERATURE
INI_TMP,         37.
**
*STEP, AMPLITUDE=STEP, INC=10000
**
** max. time increment 0.5s, so that swing of tip temp. is not too large
*COUPLED THERMAL-ELECTRICAL, DELTMX=5.0, END=PERIOD
         0.05,          720., 1e-6, 0.5
**
**
*NSET, NSET=VCC, GENERATE
       1,    2901,       1
*NSET, NSET=OUTER_TMP, GENERATE
   12367,   12367,       1
```

```
   12422,   12549,       1
   18834,   18834,       1
   18873,   18873,       1
*ELSET, ELSET=CUR_SURF
       3,       4,      310
*ELSET, ELSET=CUR_SURF_1, GENERATE
       1,       1,       1
     311,     311,       1
     314,     609,       1
*ELSET, ELSET=XXX_SUR2
   23113,   23155,   23199,    34450
*ELSET, ELSET=XXX_SUR2_1
   23075,   23113,    23155
*ELSET, ELSET=XXX_SUR2_2, GENERATE
   23076,   23112,       1
   23114,   23154,       1
   23156,   23198,       1
*NSET, NSET=COOLED, GENERATE
       1,    2901,       1
    2903,    2903,       1
    2919,    2952,       1
    7828,    7828,       1
    7846,    7890,       1
   12504,   12504,       1
   12551,   12587,       1
   18470,   18473,       1
   18475,   18573,       1
   18581,   18828,       1
   18834,   18871,       1
   18873,   18873,       1
   18911,   18913,       1
*NSET, NSET=INI_TMP, GENERATE
       1,    2917,       1
    2919,    2952,       1
    3254,    7465,       1
    7701,   12284,       1
   12367,   12549,       1
   12551,   12587,       1
   12605,   18387,       1
   18470,   18473,       1
   18475,   18573,       1
   18581,   18828,       1
   18834,   18871,       1
   18873,   18873,       1
   18911,   18913,       1
**
```

```
**
** vcc
**
*BOUNDARY, USER, OP=NEW
VCC, 9, 9,          30.
**
**NSET, NSET=TIPTMP, GENERATE
** 1,1
** 3,3
** 11,11
**
** GND
**
*BOUNDARY, OP=NEW
OUTER_TMP, 9, 9,          0.
**
** outer_tmp
**
*BOUNDARY, OP=NEW
OUTER_TMP, 11, 11,          37.
**
** cur_surf
**
*FILM, OP=NEW
**
CUR_SURF_1, F3,          33.,          1.5
CUR_SURF, F2,          33.,          1.5
**
** xxx_sur2
**
*FILM, OP=NEW
**
XXX_SUR2_1, F2,          33.,          1.5
XXX_SUR2_2, F3,          33.,          1.5
XXX_SUR2, F1,          33.,          1.5
**
** cooled
**
**DFLUX, OP=NEW
**LIVER, BFNU,          1.
**
*NODE PRINT, FREQ=1
U,
**
*OUTPUT, FIELD, VAR=PRESELECT, FREQ=1
*ELEMENT OUTPUT
```

```
ECD,FV,HFL
*NODE OUTPUT
NT, EPOT
**
**
*RESTART, WRITE, FREQUENCY=100
*END STEP
```

Appendix C

User Defined routines

```
      SUBROUTINE DFLUX(FLUX,SOL,KSTEP,KINC,TIME,NOEL,NPT,COORDS,
     1 JLTYP,TEMP,PRESS,SNAME)
C
      INCLUDE 'ABA_PARAM.INC'
C
      DIMENSION FLUX(2), TIME(2), COORDS(3)
      CHARACTER*80 SNAME
C
IF ((SOL.LT.50).AND.(SOL.GT.37)) THEN
      FLUX(1)=-4E-5*(SOL-37.0)
      FLUX(2)=-4E-5
ELSE
      FLUX(1)=0
      FLUX(2)=0
ENDIF
C
      RETURN
      END
C
      SUBROUTINE USDFLD(FIELD,STATEV,PNEWDT,DIRECT,T,CELENT,TIME,DTIME,
     1 CMNAME,ORNAME,NFIELD,NSTATV,NOEL,NPT,LAYER,KSPT,KSTEP,KINC,
     2 NDI,nshr,coord,jmac,jmtyp,matlayo,laccflg)
C
      INCLUDE 'ABA_PARAM.INC'
C
C MATERIAL AND STRENGTH PARAMETERS
      CHARACTER*80 CMNAME,ORNAME
      CHARACTER*8  FLGRAY(15)
      DIMENSION FIELD(NFIELD),STATEV(NSTATV),DIRECT(3,3),T(3,3),TIME(2),
     *  coord(*),jmac(*),jmtyp(*)
```

```
      DIMENSION ARRAY(15),JARRAY(15)
COMMON TIMOLD,UNOLD,TIPTMP,INTEG,KTIMEOLD,KCURRTIME
REAL  KDTEMP,TEMPOLD,DENSI,SPECHEAT,KTMPEPG,KTMPECD,KPERF
C
C INIT VARS
C Assuming that specific heat is constant -> Value from mat. definition
SPECHEAT=3.6
COND=0.000512
DENSI=0.00106
C DENSI=0.1
C
C FIELD(1)=ARRAY(1)
C
 CALL GETVRM('TEMP',ARRAY,JARRAY,FLGRAY,jrcd,
     $     jmac, jmtyp, matlayo, laccflg)
C STORE TEMPERATURE IN FIELD(1)
      FIELD(1)=ARRAY(1)

      IF ((FIELD(1).LT.50).AND.(FIELD(1).GT.37)) THEN
      KPERF=(-4E-5*(FIELD(1)-37.))
      ELSE
      KPERF=0
      ENDIF
C      CALCULATE DELTA TEMPERATURE
     KDTEMP=ARRAY(1)-STATEV(1)
C STORE CURRENT TEMPERATURE AS OLD TEMPERATURE FOR NEXT ITERATION
STATEV(1)=FIELD(1)
C Left Side of the term:specific heat & density is assumed constant
FIELD(2)=(KDTEMP/DTIME)*SPECHEAT*DENSI
        CALL GETVRM('EPG',ARRAY,JARRAY,FLGRAY,jrcd,
     $     jmac, jmtyp, matlayo, laccflg)
      KTMPEPG=ARRAY(1)
 CALL GETVRM('ECD',ARRAY,JARRAY,FLGRAY,jrcd,
     $     jmac, jmtyp, matlayo, laccflg)
      KTMPECD=ARRAY(1)
C FIELD(3)=ABS(FIELD(2)-(KTMPECD*(KTMPEPG)))
FIELD(3)=FIELD(2)-(KTMPECD*(KTMPEPG))-KPERF
FIELD(4)=(KTMPECD*(KTMPEPG))

 FIELD(5)=(FIELD(3)-FIELD(4))/(FIELD(3)+FIELD(4))
C
C FIELD(1): Temperature
C FIELD(2): LeftSide of the Term
C FIELD(3): gradient part   (COND TERM)
C FIELD(4): J*E
C FIELD(5):
```

```
C
C get maxnode temperature for controller: (element# NOEL, integpt# NPT (1,2 or
IF ((NOEL.EQ.5797).AND.(NPT.EQ.1)) THEN
TIPTMP=FIELD(1)
WRITE(7,*) 'TIPTMP:', TIPTMP
ENDIF
C
C
RETURN
END
C
C
C Controller
C
SUBROUTINE DISP(U,KSTEP,KINC,TIME,NODE,NOEL,JDOF,COORDS)
C
INCLUDE 'ABA_PARAM.INC'
C
DIMENSION U(3),TIME(2),COORDS(3)
C COMMON BLOCK

COMMON TIMOLD,UNOLD,TIPTMP,INTEG
C
REAL KI,KP,SETTMP,UN,DT
C
C Initialization
SETTMP=95
KP=0.27
KI=0.007
      IF (KINC.EQ.1) THEN
        INTEG=0
  UNOLD=0
  TIMOLD=0
      ENDIF
C save previous UN for comparison (see IF-THEN below)
DT=TIME(1)-TIMOLD
INTEG=INTEG+(SETTMP-TIPTMP)*DT
UN=KP*(SETTMP-TIPTMP)+KI*INTEG
IF (UN.LT.0) THEN UN=0
TIMOLD=TIME(1)
C
C only apply new voltage, if difference to previous > 0.5V, otherwise
C increment size will not increase because different voltage for each increment
C also apply new voltage if increment > 10s (so temperature swing is not too bi
C large increment times)
IF ((ABS(UN-UNOLD).GT.(0.5)).OR.(DT.GT.10)) THEN
```

```
U(1)=UN
UNOLD=UN
ELSE
U(1)=UNOLD
ENDIF
C
RETURN
END
```